

Assessing the relative impacts of satellite ozone and its precursor observations to improve global tropospheric ozone analysis using multiple chemical reanalysis systems

Takashi Sekiya¹, Emanuele Emili², Kazuyuki Miyazaki³, Antje Inness⁴, Zhen Qu⁵, R. Bradley Pierce⁶, Dylan Jones⁷, Helen Worden⁸, William Y.Y. Cheng⁸, Vincent Huijnen⁹, and Gerbrand Koren¹⁰

¹Japan Agency for Marine-Earth Science and Technology, Yokohama 2360001, Japan

²Barcelona Supercomputing Center, Barcelona, Spain

³Jet Propulsion Laboratory/California Institute of Technology, Pasadena, CA, USA

⁴European Centre for Medium-range Weather Forecasts (ECMWF), Reading, UK

⁵Department of Marine Earth and Atmospheric Sciences, North Carolina State University, Raleigh, NC 27607, USA

⁶Space Science and Engineering Center, University of Wisconsin-Madison, Madison, WI 53706, USA

⁷Department of Physics, University of Toronto, Toronto, Ontario, Canada

⁸NSF National Center for Atmospheric Research, Boulder, CO, USA

⁹Royal Netherlands Meteorological Institute (KNMI), De Bilt, the Netherlands

¹⁰Copernicus Institute of Sustainable Development, Utrecht University, Utrecht, the Netherlands

Correspondence: Takashi Sekiya (tsekiya@jamstec.go.jp)

Abstract. Chemical reanalysis products have been produced by integrating various satellite observational data to provide comprehensive information on atmospheric composition. Five global chemical reanalysis datasets were used to evaluate the relative impacts of assimilating satellite ozone and its precursor measurements on surface and free tropospheric ozone analyses for the year 2010. Observing system experiments (OSEs) ~~using the were conducted with~~ multiple reanalysis systems ~~in similar settings~~ ~~were conducted to examine under similar settings to evaluate~~ the impacts of ~~differences in reanalysis systems on observing system assessments~~ reanalysis system selection on the quantification of observing system values. Without data assimilation, large discrepancies remained among the control runs owing to model biases. Data assimilation improved the consistency among the systems, reducing the standard deviation by 72–88% in the lower troposphere through the lower stratosphere, while improving agreement with independent ozonesonde observations. The OSEs suggested the importance of precursor measurements, especially from tropospheric NO₂ columns, for improving ozone analysis in the lower troposphere, with varying influences among the systems (+increases in global lower tropospheric ozone by 0.1% in GEOS-Chem and +7% in TCR-2, with only NO₂ assimilation). Adjustments made by direct ozone assimilation showed similar vertical patterns between the TCR-2 and IASI-r systems, with increases of 6–22% and decreases of 2–21% in the middle and upper troposphere, respectively, reflecting the biases of the forecast models. These results suggest the importance of considering the effects of the forecast model performance and data assimilation configurations when assessing the observing system impacts to provide unbiased evaluations of satellite systems and to guide the design of future observing systems.

1 Introduction

Tropospheric ozone plays a key role in climate systems as a short-lived climate forcer and in tropospheric photochemistry as a determinant of oxidizing capacity and methane lifetime (Szopa et al., 2021). It is also a hazardous air pollutant that adversely affects the human health, crop productivity, and ecosystems (Fleming et al., 2018; Mills et al., 2018). Tropospheric ozone is chemically produced from precursor gases, including nitrogen oxides ($\text{NO}_x \approx \text{NO} + \text{NO}_2$), carbon monoxide (CO), and volatile organic compounds (VOCs), and it is destroyed through the chemical reaction of $\text{O}(^1\text{D})$ with water vapor. Stratosphere–troposphere ozone exchange and dry deposition at the surface are also important ozone sources and sinks, respectively.

The global tropospheric ozone distribution and its trends have been monitored in recent decades using various observation networks, including surface in-situ networks, ozonesondes, ground-based remote sensing, ~~airerafts~~[aircraft](#), and satellites (e.g., Schultz et al., 2017b; Gaudel et al., 2018; Tarasick et al., 2019). In particular, a global picture of tropospheric ozone and its precursor gases has been provided from satellite observations, such as Global Ozone Monitoring Experiment (GOME) (Burrows et al., 1999), Measurements of Pollution in the Troposphere (MOPITT) (Drummond et al., 2010), Scanning Imaging Absorption SpectroMeter for Atmospheric Chartography (SCIAMACHY) (Callies et al., 2000), Ozone Monitoring Instrument (OMI) (Levelt et al., 2006), Tropospheric Emission Spectrometer (TES) (Beer, 2006), and Microwave Limb Sounder (MLS) (Waters et al., 2006), GOME-2 (Callies et al., 2000), Infrared Atmospheric Sounding Interferometer (IASI) (August et al., 2012), and Tropospheric Monitoring Instrument (TROPOMI) (Veefkind et al., 2012). A recent study indicated ~~that~~ the complex impacts of various precursors on tropospheric ozone variability at regional to global scales ~~depend on~~ [\(Elshorbany et al., 2024\)](#). ~~Satellite HCHO and NO₂ retrievals were used to diagnose~~ ozone chemical regimes and ~~dynamical factors qualitatively, based on satellite and in-situ observations (Elshorbany et al., 2024)~~ [relate them to recent ozone increasing trends over China \(Lee et al., 2022; Ren et al., 2022\) and reversal ozone weekend effects in the US cities \(Jin et al., 2020\)](#). The combined use of satellite observations of tropospheric ozone and its precursors remains a quantitative challenge because of the non-linear transport and chemistry processes ~~involved with that impact~~ tropospheric ozone.

Several chemical reanalysis products have been developed by integrating various observational datasets with chemical transport models [\(CTMs\)](#) using data assimilation techniques. These reanalysis products provide physically and chemically consistent long-term records of atmospheric composition, including tropospheric ozone. Chemical reanalysis products have been produced using multi-species satellite observations, such as the Copernicus Atmosphere Monitoring Service (CAMS) reanalysis (CAMSRA) (Inness et al., 2019), the Tropospheric Chemistry Reanalysis version 2 (TCR-2) (Miyazaki et al., 2020a), and the Real-time Air Quality Modeling System (RAQMS) (Pierce et al., 2009). For CAMSRA and TCR-2, analyses of tropospheric ozone and related species have been validated using independent observations (Huijnen et al., 2020; Park et al., 2020; Ryu and Min, 2021). In experimental reanalysis, a smaller number of measurements are assimilated, such as tropospheric ozone in the IASI-r (Emili and El Aabaribaoune, 2021) and tropospheric NO_2 in the GEOS-Chem-adjoint systems (Qu et al., 2020).

50 The International Global Atmospheric Chemistry (IGAC) Tropospheric Ozone Assessment Report Phase II (TOAR-II) Chemical Reanalysis Focus Working Group (WG) summarizes the current status of chemical reanalysis to understand its capacity in various scientific applications. One of the important questions to be addressed is the relative impacts of individual satellite observations of stratospheric and tropospheric ozone and its precursors on surface and free tropospheric ozone analyses. Resolving this question is essential for formulating future satellite missions and comprehending our understanding of the atmospheric chemistry and climate systems. Observing system experiments (OSEs), that separately assimilate individual measurements, have been widely used in meteorological studies to optimize the data assimilation frameworks, and they have contributed to the observing system development. In atmospheric composition research, the individual impacts of satellite observations of tropospheric ozone and its precursor gases (e.g., NO₂ and CO) have been evaluated using data assimilation and chemical reanalysis frameworks (e.g., Barré et al., 2015; Miyazaki et al., 2019; Zhang et al., 2019; Emili and El Aabaribaoune, 60 2021; Inness et al., 2022; Naus et al., 2022; Sekiya et al., 2022).

Nevertheless, the implications of OSE results can be strongly affected by the the forecast model performance because of the perfect model assumption, which assumes that the forecast step within the data assimilation does not add systematic errors through model processes (Lahoz et al., 2010). Hence reanalyses inherit underlying model biases to an extent that depends on the frequency and sparseness of observations. They are also influenced by the data assimilation configurations, such as the data assimilation technique and choice of data version or satellite product level. Model-independent implications can be obtained using multi-model approaches in a common OSE framework. In a pioneering study of multi-model chemical data assimilation, Miyazaki et al. (2020b) assessed the combined impacts of assimilating multi-constituent observations into multiple models using the Multi-mOdel Multi-cOnstituent Chemical data assimilation (MOMO-Chem) framework and showed strong model dependence on emission estimates and model response to the posteriori emissions. Similarly, OSEs using a variety of chemical reanalysis systems allow for observational impact assessments that are less dependent on the characteristics of individual forecast models and data assimilation systems. Such OSE results can support the developments of chemical reanalysis and future satellite missions. 65

Therefore, based on the work of the IGAC TOAR-II Chemical Reanalysis WG activity, this study utilized five global chemical reanalysis systems, CAMSRA, TCR-2, IASI-r, GEOS-Chem, and RAQMS, to evaluate the combined and individual impacts of assimilating multiple satellite observations on tropospheric ozone analysis. Although the assimilated measurements varied between the reanalysis systems, we performed additional OSEs in closer settings across the systems to examine the relative impacts of satellite ozone and precursor measurements and their dependence on reanalysis systems. 75

The remainder of this paper is organized as follows. Section 2 describes the considered chemical reanalysis data and independent observational data for the validation. Section 3 compares the five chemical reanalysis products and validates them using independent observations. Section 4 presents the assessment results on the impacts of assimilating individual observations on tropospheric ozone analysis. Section 5 discusses future chemical reanalysis developments and satellite constellation designs. Section 6 summarizes this study. 80

2 Data

2.1 Reanalysis systems

85 Table 1 summarizes the chemical reanalysis products used in this study. Data assimilation calculations and validations were conducted for 2010, because a greater number of satellite observations were available compared with other years. Brief descriptions of these systems are provided as below.

2.1.1 CAMS reanalysis (CAMSRA)

CAMS (Peuch et al., 2022), operated by the European Centre for Medium-Range Weather Forecasts (ECMWF) on behalf of
90 the European Commission, provides daily analyses and 5-day forecasts of atmospheric composition in near-real time as well as a reanalysis of atmospheric composition going back to 2003, known as the CAMSRA (Inness et al., 2019). CAMSRA consists of three-dimensional time-consistent atmospheric composition fields, including aerosols and chemical species. It builds on the experience gained during the production of the earlier Monitoring Atmospheric Composition and Climate (MACC) reanalysis (Inness et al., 2013) and CAMS interim reanalysis (Flemming et al., 2017). Offline or reprocessed retrievals were used until
95 2016 and near-real time retrievals were used from 2017 onwards. More details can be found in Inness et al. (2019) and in the reanalysis validation reports available at <https://atmosphere.copernicus.eu/eqa-reports-global-services>.

Satellite retrievals of the total column CO, tropospheric column NO₂, aerosol optical depth, and ozone (O₃) were assimilated for CAMSRA with ECMWF's Integrated Forecasting System. The O₃ and its precursors' retrievals assimilated in CAMSRA were total column fields from SCIAMACHY, OMI, GOME-2 and TROPOMI, ozone layers from SBUV/2, ~~and stratospheric~~
100 ~~ozone profiles from MIPAS and MLS. Offline or reprocessed retrievals were used until 2016 and near-real time retrievals were used from 2017 onwards. More details can be found in Inness et al. (2019) and in the reanalysis validation reports available at <https://atmosphere.copernicus.eu/eqa-reports-global-services>.~~, total column CO from MOPITT, and tropospheric column NO₂ from OMI.

CAMSRA has a horizontal resolution of about 80 km and provides 3-hourly 3D analysis fields and forecast fields, 3-hourly
105 forecast fields as well as hourly surface forecast fields. It was produced with ECMWF's incremental 4-dimensional variational (4D-Var) data assimilation system (Courtier et al., 1994), with 12-hour assimilation windows from 09 UTC to 21 UTC and 21 UTC to 09 UTC and two minimisations at spectral truncations T95 (~210 km) and T159 (~110 km). Several atmospheric composition fields (i.e. O₃, CO, NO₂ and total aerosol mass mixing ratio) were included in the control vector and minimized together with the meteorological control variables, by adjusting the initial conditions. Emissions were not ~~optimised~~optimized.
110 The background errors for O₃ were calculated with the National Meteorological Center (NMC) method (Parrish and Derber, 1992) and are univariate; i.e. the error covariance matrix between ozone and the other chemical and dynamical fields is diagonal.

The descriptions of the CTM applied in CAMSRA are given by Flemming et al. (2015). The chemical mechanism of the IFS used in CAMSRA was a modified and extended version of the CB05 (Yarwood et al., 2005) chemical mechanism for the troposphere, as implemented in the ~~chemical transport model (CTM)~~ CTM TM5 (Huijnen et al., 2010). CB05 describes the
115 tropospheric chemistry with 55 species and 126 reactions. Stratospheric ozone chemistry was parameterized by a "Cariolle-

scheme” (Cariolle and Déqué, 1986; Cariolle and Teysse re, 2007). Ozone and aerosol fields were used interactively in the numerical weather prediction (NWP) radiation scheme of CAMSRA.

The [a priori](#) anthropogenic emissions used in CAMSRA came from the MACCity inventory (Granier et al., 2011), with modifications to increase winter-time road traffic emissions over North America and Europe following the correction of Stein et al. (2014). Biomass burning emissions were taken from the Global Fire Assimilation System (GFAS v1.2; Kaiser et al., 2012). Monthly mean biogenic emissions simulated by the MEGAN2.1 model following Sindelarova et al. (2014) were used for the period 2003–2017, and in the later years a monthly-mean climatology derived from the 2003–2017 simulations was applied.

The validation in Inness et al. (2019) showed that the CAMSRA has smaller biases compared with observations than the previous two reanalyses (MACC and CAMS interim) and is more consistent in time, especially compared to the MACC reanalysis (e.g., Inness et al., 2019; Wagner et al., 2021). Evaluation of more recent years can be found in the validation reports at <https://atmosphere.copernicus.eu/eqa-reports-global-services>. In addition to CAMSRA, CAMS also produced a control run which used the same meteorology as CAMSRA but did not assimilate any atmospheric composition data.

2.1.2 TCR-2

[Tropospheric Chemistry Reanalysis version 2 \(TCR-2\) provides both emissions and atmospheric abundance of various chemical species from the assimilation of multi-constituent measurements from multiple satellite instruments during 2005–2021 \(Miyazaki et al., 2020a\). This reanalysis products were developed under the Multi-mOdel Multi-cOnstituent Chemical data assimilation \(MOMO-Chem\) framework \(Miyazaki et al., 2020b\).](#)

The TCR-2 products ([Miyazaki et al., 2020a](#)) were obtained from the assimilation of the OMI, SCIAMACHY, GOME-2 NO₂ QA4ECV v1.1 products (Boersma et al., 2017a, b, c), the TES V6 ozone profile, the MLS v4.2 ozone and HNO₃ (Livesey et al., 2018), the MOPITT CO v7 TIR/NIR product (Deeter et al., 2017), and the OMI PBL SO₂ product (Li et al., 2013). ~~The reanalysis calculation was conducted at~~

~~The TCR-2 has a horizontal resolution of T106 (~1.1° × 1.1°) with 32 vertical layers up to an altitude of 40 km using the MIROC-Chem global chemical transport model (Sekiya et al., 2018) and an ensemble Kalman filter (EnKF) technique.~~

~~The forecast model calculates tracer transport, emissions, deposition, and chemical processes, including the ozone–CO–VOCs system (92 chemical species and 262 chemical reactions). The meteorological fields calculated in the dynamical and physical modules of MIROC-Chem were nudged to the 6-hourly ERA-Interim reanalysis (Dee et al., 2011) and used in the chemical module at every model time step (4–8 min).~~

~~The TCR-2 reanalysis system employs the local ensemble transform Kalman filter (LETKF) technique (Hunt et al., 2007). The state vector includes the surface emissions of NO_x, CO, and SO₂, and lightning NO_x sources, as well as the concentrations of 35 chemical species. Surface and lightning emissions were estimated based on a state argumentation method (e.g., Evensen, 2009), which used the relationship between emissions and concentrations in the background error covariance matrix generated based on ensemble model simulations. In the analysis step, the standard deviation of the emission ensembles was inflated to a~~

predefined minimum value obtained through sensitivity calculations (i.e., 56% of the a priori emissions) to prevent covariance underestimation.

The CTM used in TCR-2 was MIROC-Chem (Sekiya et al., 2018), which calculates tracer transport, emissions, deposition, and chemical processes, including the ozone-HO_x-NO_x-CO-VOCs system (92 chemical species and 262 chemical reactions). The meteorological fields calculated in the dynamical and physical modules of MIROC-Chem were nudged to the 6-hourly ERA-Interim reanalysis (Dee et al., 2011) and used in the chemical module at every model time step (4–8 min).

A priori emissions were obtained from the HTAP v2.2 inventory for the anthropogenic sources (Janssens-Maenhout et al., 2015) and the GFED v4.1 inventory for the biomass burning (Randerson et al., 2018), while those from soil NO_x were based on the GEIA inventory (Graedel et al., 1993).

A control model simulation without any data assimilation, which was evaluated by Miyazaki et al. (2020a), was used as the baseline in this study.

2.1.3 IASI-r

IASI-r (Emili and El Aabaribaoune, 2021) is a year long reanalysis experiment conceived to demonstrate the added value of assimilating ozone sensitive infrared measurements from the Infrared Atmospheric Sounding Interferometer (August et al., 2012). It was prepared based on previous experience in assimilating IASI Level 2 ozone retrievals (Emili et al., 2014; Peiro et al., 2018) and Level 1 radiances (Emili et al., 2019; Aabaribaoune et al., 2021) ~~for 2010.~~

~~The chemical transport model being used was MOCAGE (Josse et al., 2004), and it was setup on a 2x2 degrees global grid with 60 vertical levels up to 0.1 hPa and using meteorological forcing from ERA-interim (Dee et al., 2011). The IASI-r configuration employs a linearized ozone chemistry thorough the entire atmosphere (Cariolle and Teysse, 2007), with the ozone in the middle and lower troposphere being relaxed to a static zonal climatology. This relatively light model configuration is meant to run long term ozone reanalyses (Peiro et al., 2018), with assimilated observations providing the main spatio-temporal constraint on tropospheric ozone distribution.~~

IASI-r assimilates both ozone-sensitive radiances (Level 1) from IASI (980-1100 cm⁻¹) and stratospheric level 2 profiles from the Microwave Limb Sounder (MLS).

The IASI-r has 2° × 2° global grid with 60 vertical levels up to 0.1 hPa. The reanalysis was conducted using a 3-dimensional variational (3D-Var) data assimilation algorithm and hourly windows. Background and observation error covariances were either diagnosed (Aabaribaoune et al., 2021) or specified as a function of the vertical layer, tropopause height, and local ozone concentration (Emili and El Aabaribaoune, 2021). With the given setup, only ozone concentrations can be corrected by the data assimilation. Due to the limited vertical sensitivity of the assimilated observations and the simplified model configuration, little information is provided by IASI-r on ground-level ozone. Hence, the main target of IASI-r is ozone in the free and upper troposphere.

The CTM being used was MOCAGE (Josse et al., 2004), and it was using meteorological forcing from ERA-interim (Dee et al., 2011). The IASI-r configuration employs a linearized ozone chemistry thorough the entire atmosphere (Cariolle and Teysse, 2007), with the ozone in the middle and lower troposphere being relaxed to a static zonal climatology. This relatively light model

configuration is meant to run long term ozone reanalyses (Peiro et al., 2018), with assimilated observations providing the main spatio-temporal constraint on tropospheric ozone distribution.

185 2.1.4 GEOS-Chem

We used the GEOS-Chem adjoint model (Henze et al., 2007) v35k at the $2^\circ \times 2.5^\circ$ resolution to assimilate tropospheric NO₂ observations from OMI and simulate global ozone concentrations using the ~~posterior a posteriori~~ NO_x emissions ~~at the $2^\circ \times 2.5^\circ$ resolution~~ for 2005–2016. ~~The GEOS-Chem model is driven by the Modern-Era Retrospective analysis for Research and Applications, Version 2 (MERRA-2) meteorological fields from the NASA Global Modeling and Assimilation Office (GMAO). Prior anthropogenic emissions of , , , (non-methane volatile organic compounds), and primary aerosols were obtained from the HTAP 2010 inventory version 2 (Janssens-Maenhout et al., 2015). We also obtained 3-hourly wildfire emissions from GFED4 (Giglio et al., 2013). The other emissions and setups follow those of Qu et al. (2017, 2019a, b, 2020).~~

190 The OMI Level 2 NO₂ retrieval from the NASA product OMNO2 version 3 (Krotkov et al., 2017) was used for the assimilation. We screened all OMI NO₂ retrievals using data quality flags and by the criteria of positive tropospheric column, cloud fraction of < 0.2 , solar zenith angle $< 75^\circ$, and viewing zenith angle of $< 65^\circ$. All retrievals that are affected by row anomalies were excluded. GEOS-Chem NO₂ vertical column densities (VCDs) were converted to slant column densities (SCDs) using scattering weight from the OMI retrievals and then compared the GEOS-Chem SCDs with the SCDs retrieved from OMI.

195 The OMI NO₂ retrievals were assimilated using the hybrid 4D-Var/mass balance inversion of NO_x emissions as described in Qu et al. (2017). A cost function was defined as the observation-error-weighted differences between the simulated and retrieved NO₂ SCDs plus the prior emissions error-weighted departure of the emission scaling factors from the prior estimates. The GEOS-Chem adjoint model minimizes the cost function using the quasi-Newton L-BFGS-B gradient-based optimization technique (Byrd et al., 1995; Zhu et al., 1994), in which the gradient of the cost function with respect to the control parameter is calculated using the adjoint method. Details of the assimilation of NO₂ SCDs, how vertical sensitivities of satellite retrievals are accounted for, ~~and the hybrid 4D-Var/mass balance inversion.~~

205 The GEOS-Chem model is used as CTM, which is driven by the Modern-Era Retrospective analysis for Research and Applications, Version 2 (MERRA-2) meteorological fields from the NASA Global Modeling and Assimilation Office (GMAO).

A priori anthropogenic emissions of NO_x emissions are described in Qu et al. (2017). ~~SO₂, NH₃, CO, NMVOCs (non-methane volatile organic compounds), and primary aerosols were obtained from the HTAP 2010 inventory version 2 (Janssens-Maenhout et al., 2015). We also obtained 3-hourly wildfire emissions from GFED4 (Giglio et al., 2013). The other emissions and setups follow those of Qu et al. (2017, 2019a, b, 2020).~~

2.1.5 RAQMS

The ~~RAQMS chemical reanalysis~~ Real-time Air Quality Modeling System (RAQMS) chemical reanalysis (Pierce et al., 2009; Bruckner et al. uses satellite trace gas and aerosol retrievals from the NASA satellites (Terra, Aqua, and Aura) covering 2006 through 2016.

215 ~~The operational grid point statistical interpolation (GSI) 3d-variational-analysis system (Wu et al., 2002) was used to assimilate retrievals-~~

The assimilated retrievals were obtained from the Aura Ozone Monitoring Instrument (OMI) cloud cleared total column ozone (McPeters et al., 2008), Microwave Limb Sounder (MLS) (Froidevaux et al., 2008) stratospheric ozone profiles, OMI tropospheric column NO₂ (Boersma et al., 2007), Terra and Aqua Moderate Resolution Imaging Spectrometer (MODIS) aerosol optical depth (AOD) (Remer et al., 2005), and Atmospheric Infrared Sounder (AIRS) carbon monoxide (Yurganov et al., 2008).

RAQMS chemical reanalysis has a horizontal resolution of 1° × 1° and uses the operational grid point statistical interpolation (GSI) 3-D variational analysis system (Wu et al., 2002) at three-hour intervals for the assimilation. Analysis increments from the OMI tropospheric column NO₂ assimilation were used for off-line adjustment ~~of the a priori 2010 Hemispheric Transport of Air Pollution (HTAP, 2010) anthropogenic emission inventories~~ following an offline mass balance approach similar to East et al. (2022). ~~RAQMS biomass burning emissions used Terra and Aqua MODIS fire detections following Soja et al. (2004)~~

The CTM used in the reanalysis was RAQMS. The dynamical core of RAQMS is the UW-Hybrid model (Schaack et al., 2004). RAQMS-Aura meteorological predictions were initialized at 6-hour intervals with archived analyses from the National Center for Environmental Prediction (NCEP) Global Data Assimilation System (GDAS) (Kleist et al., 2009).

230 The a priori emissions were taken from the 2010 Hemispheric Transport of Air Pollution (HTAP, 2010) anthropogenic emission inventories. RAQMS biomass burning emissions used Terra and Aqua MODIS fire detections following Soja et al. (2004)

~

2.2 Observing system experiments (OSEs)

The assimilated measurements were largely different among the systems, which increased the ~~difficulty~~-difficulty of implementing common OSE settings. The categorization of the assimilated measurements can be simplified into the three groups: stratospheric ozone (S), including total ozone column retrievals derived from backscatter ultraviolet (UV) instruments and ozone profile retrievals using microwave instruments; tropospheric ozone (T), consisting of ozone profiles obtained from infrared (IR) instruments; and ozone precursors (P), including tropospheric NO₂ column retrievals from UV/visible sensors and total CO column and profile retrievals derived from IR instruments. As summarized in Table 2, five chemical reanalysis datasets and additional OSEs were divided into the following three types: (1) simultaneous assimilation of ozone and its precursors (S+T+P and S+P), (2) direct ozone assimilation (S+T, S, and T), and (3) assimilation of ozone precursor gases such as NO₂ and CO (P). We also performed OSEs using the TCR-2 and IASI-r chemical reanalysis systems, including four TCR-2 OSEs that assimilated MLS stratospheric ozone and HNO₃ profiles (hereinafter TCR-2-S, type 2), TES tropospheric ozone profile (TCR-2-T, type 2), OMI, SCIAMACHY, and GOME-2 NO₂ (TCR-2-P_NO₂, type 3), and MOPITT CO (TCR-2-P_CO, type 3); and an IASI-r OSE for the IASI L1 radiance sensitive to tropospheric ozone profile (IASI-r-T, type 2).

2.3 Validation data

2.3.1 OMI-MLS satellite observations

For the validation, we used global distributions of the tropospheric ozone column (TOC) derived from OMI-MLS (Ziemke et al., 2006), which is a relatively independent data product that was not used in three of the chemical reanalysis systems
250 (~~but both~~ although both the OMI total ozone column and MLS ozone profiles were assimilated in CAMSRA and RAQMS) and covers the period when all the reanalysis datasets and control simulations were available. The TOC from OMI-MLS was produced using the tropospheric ozone residual method, which subtracted the MLS stratospheric ozone column from the OMI total ozone column. The OMI-MLS TOC was derived using tropopause pressure determined from NCEP analyses with the 2 K km⁻¹ vertical temperature gradient criterion of the World Meteorological Organization (WMO). The 1 σ precision for the
255 monthly-mean TOC was estimated to be approximately 1.3 DU (Ziemke et al., 2019). For comparison with the OMI-MLS TOC, the same tropopause data from NCEP analyses were applied to the chemical reanalysis products.

2.3.2 Ozonesonde observations

The vertical profiles of the ozone analyses were validated against independent ozonesonde observations obtained from the World Ozone and Ultraviolet Data Center (WOUDC; <http://www.woudc.org>). The measurement precision was better than
260 5%, and the accuracy was within 5–10% (Smit et al., 2007). We used 261 profiles for the northern high latitudes (60–90°N), 1284 profiles for the northern mid-latitudes (30–60°N), 349 profiles for the tropics (30°N–30°S), 123 profiles for the southern mid-latitudes (30–60°S), and 196 profiles for the southern high latitudes (60–90°S) from 2010. The observed and analyzed vertical profiles were compared at ozonesonde locations in the 29 vertical pressure bins from 1013.25 to 70 hPa. The validation was conducted against ozonesonde observations collected for five latitude bands to evaluate the global reanalysis performance in a manner that reflects regional characteristics. This approach was chosen instead of evaluating reanalysis performance at individual observation sites, which can be influenced by sparse temporal sampling, limited spatial coverage, and the influence of local processes. Aggregating individual ozonesonde sites with similar characteristics provide a more representative view of larger regions, as demonstrated by Tilmes et al. (2012). However we acknowledge that the number of observations within each latitudinal band may not always be sufficient to fully capture regionally representative model
265 performance (Miyazaki and Bowman, 2017) or to accurately evaluate long-term trends (Chang et al., 2024).
270

2.3.3 Surface in situ observations

The TOAR global surface ozone database (~~Schultz et al., 2017b~~) (Schultz et al., 2017a, b) for 2010 was used to evaluate the surface ozone analyses. A globally consistent TOAR database was constructed by combining almost 10,000 sites, characterizing the measurement sites, and applying consistent quality control. The total uncertainty in modern ozone measurements
275 (1990–2014) at a mean level of 30 nmol mol⁻¹ was estimated at <2 nmol mol⁻¹ (Tarasick et al., 2019). The TOAR database provides annual, seasonal, and monthly statistics for both urban and rural sites. All the reanalysis systems have relatively coarse

horizontal resolutions; therefore, they can not resolve ozone variability in urban areas. Thus, we used $2^\circ \times 2^\circ$ monthly-mean ozone concentrations at the rural sites in 2010. For the comparison, ~~all the~~ ozone analysis fields in CAMSRA and TCR-2 were regridded from ~~the original~~ their original model grid points onto a $2^\circ \times 2^\circ$ grid using inverse distance weighting, while those in
280 GEOS-Chem and RAQMS were regridded using bilinear interpolation.

3 Comparison of multiple chemical reanalysis products

3.1 Data assimilation impacts

Figure 1 presents the vertical and latitudinal distributions of annual mean ozone concentrations obtained from the chemical reanalysis products, control runs, and their differences for 2010. Large discrepancies in ozone concentrations between different
285 models were found in the lower stratosphere and troposphere, with the standard deviations of 27% in the global mean in the upper troposphere and lower stratosphere (UTLS, 70–250 hPa), 8% in the middle troposphere (400–600 hPa), and 9% in the lower troposphere (below 800 hPa).

Data assimilation increased the annual mean ozone concentrations in the UTLS in 2010 by 10–40% in CAMSRA and by more than 100% in RAQMS, except in the tropics, and it decreased the concentrations by 5–30% in TCR-2 and IASI-r. In the
290 middle troposphere, data assimilation increased the global mean ozone in all the reanalysis products in most cases, with larger increases in TCR-2, IASI-r, and RAQMS (by 15–50%) than in CAMSRA ~~and GEOS-Chem~~ (by up to 5%). This discrepancy reflects the large inter-system differences in assimilation increments over the tropics. In the lower troposphere, data assimilation increased the ozone concentration by 5–30% in CAMSRA, TCR-2, and RAQMS, whereas it only had minor impacts ($< 5\%$)
295 ~~in IASI-r~~ and. Data assimilation in GEOS-Chem adjoint has a minimal impact on free tropospheric ozone compared to the other systems. Data assimilation also improved the consistency in ozone concentrations among the multiple systems, with the standard deviation of the global mean ozone between different reanalysis systems reduced to 3.2% in the UTLS, 1.7% in the middle troposphere, and 2.5% in the lower troposphere.

Similar reductions in the multi-model spread were observed for near-surface ozone (Fig. 2). The standard deviations of the control runs were 22%, 11%, and 14% for the southern extratropics ($25^\circ\text{--}90^\circ\text{S}$), the tropics ($25^\circ\text{N--}25^\circ\text{S}$), and the northern
300 extratropics ($25^\circ\text{--}90^\circ\text{N}$), respectively. Data assimilation increased the near-surface annual mean ozone by 2–8 nmol mol^{-1} in CAMSRA, TCR-2, and RAQMS. The impact of assimilation on surface ozone was small in the IASI-r and GEOS-Chem. Data assimilation reduced the standard deviation of ozone analyses between the reanalysis systems to 14%, 6%, and 11% over the southern extratropics, tropics, and northern extratropics, respectively.

3.2 Validation using independent observations

3.2.1 OMI-MLS satellite observations

305

Figure 3 compares the ~~tropospheric ozone column (TOC)~~ TOC between the chemical reanalysis products and control runs with OMI-MLS TOC observations. All the control runs captured the observed general features. However, the CAMSRA and

310 GEOS-Chem control runs underestimated the TOC near 60°N and 60°S by up to 10 DU and overestimated the TOC from the tropics to the subtropics in both hemispheres by 5–10 DU. In contrast, the TCR-2 control run overestimated the TOC over the northern mid-latitudes by approximately 5 DU and the IASI-r control run overestimated the TOC over the southern mid-latitudes by 2–4 DU, whereas both models underestimated the TOC over the tropics and subtropics by 5–15 DU. The RAQMS control run overestimated the TOC over the tropical land areas and the Atlantic by approximately 5 DU and underestimated the TOC over the Pacific and the Southern Oceans by up to 10 DU. The spatial correlation coefficients of the observed vs. simulated TOC ranged from 0.69 to 0.89.

315 After data assimilation, all ~~the~~ chemical reanalysis products ~~commonly consistently~~ revealed positive biases of 5–10 DU relative to OMI-MLS from the tropics to the mid-latitudes of both hemispheres. However, ~~the~~ this result is inconsistent with the reanalysis comparison results against ozonesonde measurements (see Section 3.2.2). Considering ozonesonde measurements as ground truth, part of the positive bias relative to OMI-MLS can be attributed to smaller TOC in the OMI-MLS data (by 3.7 DU on average) compared to ozonesonde observations, as confirmed in Figure 3 and reported by Gaudel et al. (2024). Data
320 assimilation improved the spatial correlation coefficients ~~were improved to~~ > 0.83 ~~in all the systems. Thus, good consistency was observed among the reanalysis products~~ for all systems, demonstrating the usefulness of the reanalysis products and the value of the OMI-MLS data for the evaluation of TOC spatial distributions. The remaining ~~biases in the reanalysis products indicate the difficulty of correcting tropospheric ozone through data discrepancies~~ underscore the challenges in improving tropospheric ozone analyses through the assimilation of precursors ~~and stratospheric profiles or column measurements of ozone~~
325 , stratospheric profiles, or column ozone measurements. This could be related to model errors near the surface (e.g., excessive chemical production of ozone from precursors) ~~, differences in procedures for computing TOC between the observations and models (e.g., vertical discretization around the tropopause), and positive biases of OMI-MLS against ozonesonde observations (Gaudel et al., 2024).~~ In the IASI-r and positive biases in the assimilated tropospheric ozone retrievals (Boxe et al., 2010) in the TCR-2 ~~systems,~~ in which tropospheric ozone profiles were assimilated. ~~However, common positive biases against OMI-MLS~~
330 ~~can partly be affected by positive biases in the assimilated tropospheric ozone retrievals (Boxe et al., 2010; Dufour et al., 2012)~~ Vertical resolution of the compared data differed largely around the tropopause (i.e., MLS resolution of 2–3 km and model resolution of < 1 km), which can affect the computation of TOC when a sharp ozone gradient occurs and may lead to discrepancy in the comparison (Schoeberl et al., 2007).

3.2.2 Ozonesondes

335 Figure 4 presents the vertical distributions of mean biases and root-mean-square errors (RMSEs) for the reanalysis products and control runs relative to ozonesonde observations, over five latitude bands in 2010. As summarized in Table 3, in the UTLS (70–250 hPa), large positive and negative ozone biases in the control runs varied among the models over all the latitude bands. As shown in Figures 5 and S1, over the northern mid and high latitudes, RAQMS showed larger seasonal amplitudes in model bias, with a maximum in boreal spring, compared with the other forecast models. Over the southern mid and high latitudes,
340 CAMS and RAQMS showed larger negative biases in austral summer and fall compared to other models, while TCR-2 and

IASI-r exhibited maximum positive biases in austral spring. The multi-model average RMSE against ozonesonde observations was $55\pm 17\%$ globally (44–61% for the five latitude bands).

In the middle troposphere (400–600 hPa), the model biases in the control runs were negative over the southern mid-latitudes and the northern mid-latitudes and high latitudes, whereas the biases varied among the models over the southern high latitudes and the tropics. The seasonal variations of model biases were approximately 20% larger in IASI-r compared to the other models. IASI-r showed maximum negative biases over the northern midlatitudes and maximum positive biases over the southern high latitudes during summer. Moreover, the multi-model average RMSE was $28\pm 4\%$ (25–34% between the different latitude bands).

In the lower troposphere (800–900 hPa), model biases in the control runs differed between models over the southern mid-latitudes, high latitudes, and tropics, whereas the model biases were commonly negative over the northern mid-latitudes and high latitudes. IASI-r exhibited larger biases compared to the other models over the mid and high latitudes in summer in both hemispheres, whereas RAQMS and TCR-2 showed larger negative biases over the mid and high latitudes in winter in both hemispheres. The RMSE for ozone obtained from the multiple forecast models was $27\pm 5\%$ (20–43% over the five latitude bands).

Data assimilation reduced the mean biases in the UTLS to -3 to 9% over all the latitude bands relative to the control runs. Over the tropics, the mean bias in TCR-2 was increased by 3% owing to data assimilation. Nevertheless, large positive and negative biases above and below 150 hPa were largely reduced by data assimilation, compared to the control runs in TCR-2. Seasonally dependent biases were also improved by data assimilation over all the latitude bands. Data assimilation decreased the RMSEs of the multi-system mean and spread obtained from the reanalysis systems to $30\pm 7\%$ relative to global ozonesonde observations in the UTLS (18–40% over the five latitude bands).

In the middle troposphere, data assimilation increased the mean biases to 5–15% in TCR-2, IASI-r, and RAQMS over the southern high latitudes relative to the control runs, although it decreased the mean biases in CAMSRA to less than 2%. Data assimilation also reduced the mean biases over the southern mid-latitudes (except for IASI-r), the tropics, and the northern mid-latitudes and high latitudes. The seasonal variations in model biases were also reduced. However, multi-system ~~RMSE~~ mean and spread mean biases in winter remained over the high latitudes in both hemispheres, likely due to the limited number of assimilated observations in these regions during winter. The multi-system mean and spread of RMSE were also decreased by data assimilation to $23\pm 3\%$, compared to the control runs over the globe (21–28% over all the latitude bands).

In the lower troposphere, in contrast to the middle troposphere, the mean biases in TCR-2, IASI-r, and RAQMS were reduced by up to 88% over the southern high latitudes, compared to the control runs, while the mean bias in CAMSRA was increased. Over the tropics, data assimilation increased the mean biases by 54% in TCR-2 and a factor of 4.4 in RAQMS. Over the southern mid-latitudes and northern mid-latitudes and high latitudes, data assimilation decreased the mean biases in all the reanalysis systems. In these regions, the seasonal dependency of model biases was not improved by data assimilation. The multi-system RMSE mean and spread were also reduced to $25\pm 5\%$ compared to global ozonesonde observations (18–42% over all the latitudes bands).

Figure 6 shows the model biases of the annual mean surface ozone against the TOAR database (Schultz et al., 2017b) (Schultz et al., 2017a, over the United States, Western Europe, and Northeast Asia for 2010. Over the United States, the control runs showed positive biases relative to the TOAR database, ranging from 2.4 to 16.2 nmol mol⁻¹. The spatial correlation coefficients and RMSEs in the control runs were 0.13–0.54 and 5.3–16.7 nmol mol⁻¹ compared to the TOAR database, respectively. After data assimila-
380 tion, the positive model biases were increased by up to a factor of 2.5. The spatial correlation coefficients were decreased by 0.01–0.05, except for TCR-2, whereas the RMSEs were increased by up to 31%.

Over Western Europe, surface ozone model biases in the control runs were 2.5–15.1 nmol mol⁻¹ relative to the TOAR database. The spatial correlation coefficients and RMSEs were 0.37–0.55 and 5.7–15.8 nmol mol⁻¹ compared to the TOAR database, respectively. Data assimilation increased the positive model biases by a factor of up to two. The spatial correlation
385 coefficients were slightly decreased by 0.005–0.01 in CAMSRA and GEOS-Chem, whereas the spatial correlation coefficients were increased by 0.02–0.06 in TCR-2 and RAQMS. The RMSEs were increased by 1–35%.

Over Northeast Asia, surface ozone model biases in the control runs were positive (4.2–17.8 nmol mol⁻¹) compared to the TOAR database. The spatial correlation coefficients ranged from 0.01 to 0.5 among the models. The RMSEs against the TOAR database were 7.6–18.8 nmol mol⁻¹. Through data assimilation, the model biases were increased by up to 42% in all
390 the systems. The spatial correlation coefficients were decreased by 0.03 in RAQMS but improved by 0.02–0.07 in CAMSRA, TCR-2, and GEOS-Chem. The RMSEs were increased by up to 23% for all the systems.

Overall, the positive model bias of surface ozone against all available observations (0.3–12.8 nmol mol⁻¹) was increased by data assimilation by up to a factor of 4. The spatial correlation coefficients were slightly decreased by data assimilation from 0.11–0.59 to 0.08–0.58, except for TCR-2. The RMSEs were increased by up to 18% for all the reanalysis products. Satellite
395 data assimilation reduced negative model biases in the free troposphere, whereas propagation of the ozone increments to the surface increased surface ozone biases. These results indicate a misrepresentation of physical and chemical model processes near the surface in the current global forecast models (Parrington et al., 2009; Travis et al., 2016) and highlight the need to incorporate surface observations into the current global chemical reanalysis data (Hanea et al., 2004; Huang et al., 2013).

4 Relative impacts of satellite ozone and its precursor observations

400 4.1 OSE results

OSEs were used to evaluate the relative impacts of individual assimilated measurements, as summarized in Table 2. In particular, we focused on three groups: (1) simultaneous assimilation of ozone and its precursors (S+T+P or S+P), (2) direct assimilation of stratospheric and tropospheric ozone (S+T, S, or T), and (3) assimilation of ozone precursors including NO_x and CO on ozone analysis (P(NO₂) or P(CO)). As shown in Figs. 1, 2, 7, and 8, the effects of assimilation varied from system to
405 system. Nevertheless, similarities in the general patterns were observed. System-dependent differences in ozone increments can

be attributed to differences in model biases, data assimilation configurations (e.g., concentration and/or emission optimization), and assimilated measurements.

For the simultaneous assimilation cases (S+T+P or S+P), in the UTLS, the global mean ozone concentrations increased in CAMSRA (S+P) and RAQMS (S+P) by 18–61% but decreased in TCR-2 (S+T+P) by 21%. The discrepancy in the
410 increments reflects opposite model biases (c.f., Section 3.2.2). In the middle and lower troposphere, ozone concentrations commonly increased over the extratropics but varied in magnitudes, ranging from 3% (CAMSRA) to 20% (TCR-2). Increases in ozone near the surface were also common, with larger increases over remote areas than over the polluted and biomass-burning areas. The increases in ozone concentrations obtained from the systems with emission optimization (by 11–27% in TCR-2 and RAQMS) tended to be larger than those without optimization (by 4–11% in CAMSRA).

415 The direct ozone assimilation cases (S+T, S, or T) showed similar latitudinal and vertical patterns in the effects of data assimilation in the middle to upper troposphere (Fig. 7), reflecting similar model biases in the MIROC-Chem and MOCAGE models. The maximum changes in the tropical middle and lower troposphere was more than 40%. TCR-2-S (S), TCR-2-T (T), IASI-r (S+T), and IASI-r-T (T) increased the ozone concentration in the middle troposphere (by 6–22%) and decreased it in the UTLS (by 2–21%). Decreases in UTLS ozone in the assimilation of stratospheric ozone profiles (TCR-2-S (S) and
420 IASI-r (S+T)), were commonly larger than those in the assimilation of tropospheric ozone only (TCR-2-T (T) and IASI-r-T (T)). The effects on the tropical lower stratosphere and lower troposphere differed between TCR-2 and IASI-r. These different patterns may reflect differences in assimilated observations (TES vs. IASI) as well as model biases. Near the surface, direct ozone assimilation in TCR-2 showed large data assimilation impacts of up to 7%, 13%, and 8% in the southern extratropics, tropics, and northern extratropics, respectively (Fig. 8). The surface ozone change was smaller in IASI-r than TCR-2, partly
425 because the prescribed background error covariance ~~(by in IASI-r (10%) in IASI-r in the lower troposphere was smaller than the ensemble spread of the ozone first guess (typically by was lower than the typical background error in TCR-2 (15–17%) in the lower troposphere. In TCR-2, the background error covariance was dynamically estimated through ensemble model simulations at each location and time, which is expected to provide more accurate estimates of background error.~~ Other reasons for significant differences near the surface could be related to the altitude-dependent sensitivities of the assimilated observations
430 (i.e., averaging kernels).

The assimilation of ozone precursor gases (P(NO₂) or P(CO)) increased the ozone concentrations in the lower and middle troposphere in the OSEs using TCR-2 and GEOS-Chem. The TCR-2 OSE results indicated a larger impact on the surface and lower tropospheric ozone from the assimilation of NO₂ (by +7%) than from the assimilation of CO (by +1.5%). The impacts of tropospheric NO₂ assimilation varied among the systems, ranging from 0.1% (GEOS-Chem) to 7% (TCR-2). This discrepancy
435 may be related to the smaller increments in NO_x emissions in the GEOS-Chem adjoint calculation when assimilating the OMNO2 NASA standard product than those when assimilating the DOMINO and QA4ECV products (Qu et al., 2020). This discrepancy can also be caused by the different sensitivities of ozone to changing NO_x emissions between GEOS-Chem and MIROC-Chem (Miyazaki et al., 2020b) and the simultaneous corrections of NO_x emissions and concentrations in TCR-2 (Miyazaki et al., 2012b). Meanwhile, the positive responses of ozone to MOPITT CO assimilation were consistently reported
440 by Gaubert et al. (2016).

4.2 Validation against ozonesonde observations

As shown in Figs. 9 and 10, the chemical reanalysis products and OSEs were validated using ozonesonde observations. In the extratropical UTLS, model biases were largely reduced by more than 67% by the simultaneous assimilation in CAMSRA (S+P), TCR-2 (S+T+P), and RAQMS (S+P). Over the tropics, model biases were also reduced by up to 74% in the lower
445 stratosphere (70–150 hPa) and 44% in the upper troposphere (150–250 hPa), respectively (Fig. 10). The OSEs suggested the importance of the direct assimilation of stratospheric ozone profiles in IASI-r (S+T) and TCR-2-S (S), with bias reductions of 73–95% over the extratropics. Although the mean bias in the tropical UTLS (70–250 hPa) was increased in TCR-2-S, the positive and negative biases were improved by 60% in the lower stratosphere and by 86% in the upper troposphere.

In the middle troposphere, the model bias was reduced by 88% in CAMSRA (S+P) over the southern high latitudes, whereas
450 it was increased by 3–21% in TCR-2 (S+T+P) and RAQMS (S+P). Over the other four latitude bands, the simultaneous assimilation (S+T+P or S+P) improved the model biases compared to ozonesonde by 24–99%. The direct ozone assimilation of TES tropospheric ozone profile in TCR-2-T (T) showed bias reductions of 67% and 89% over the southern mid- and high latitudes, respectively. In contrast, model biases were increased by the IASI tropospheric ozone assimilation in IASI-r (S+T). Over the tropics, the model biases were reduced by 45–73% in TCR-2-T (T) and IASI-r (S+T) in the northern mid-latitudes
455 and high latitudes. The assimilation of ozone precursor measurements in TCR-2-P_NO_x and TCR-2-P_CO (P) reduced the model biases by 34–97% over all the latitude bands, with the exception of TCR-2-P_CO over the southern high latitudes.

In the lower troposphere, the simultaneous assimilation reduced the model biases over the southern high latitudes by up to 88% in TCR-2 (S+T+P) and RAQMS (S+P), except for CAMSRA (S+P). Over the tropics, the CAMSRA remained essentially unchanged (by 2%), whereas the other simultaneous assimilations increased model biases. Over the southern mid-
460 latitudes, and northern mid-latitudes and high latitudes, all the simultaneous assimilation (S+T+P and S+P) reduced the negative model biases by 24–81%. Over the extratropics, the direct tropospheric ozone assimilation (S+T and T) reduced the model biases by up to 82%. Compared with these improvements, the assimilation of precursor measurements (P) showed comparable or larger bias reductions of 33–90% over the extratropics. Over the tropics, however, improvements in model biases were not found for the direct ozone assimilation or precursor assimilation (S+T, T, and P), except for IASI-r (by 59%).
465 These results could partly be affected by biases in the assimilated measurements (Boxe et al., 2010), a lack of observational constraints on biogenic VOCs (De Smedt et al., 2018; Wells et al., 2022), and missing model processes, such as tropospheric halogen chemistry (Sherwen et al., 2016; Sekiya et al., 2020).

5 Discussion

The results obtained from multi-system OSEs have two important implications for the development of a future satellite con-
470 stellations ~~. Multi-system OSE comparisons broadly suggested that integrating as follows: (1) Integrating~~ measurements of ozone and its precursors is an effective way to improve the entire profile of ozone in the troposphere and lower stratosphere. ~~This has been commonly~~, as consistently suggested by previous single-system OSE studies (e.g., Miyazaki et al., 2019); ~~and indicates~~. This finding highlights the great value of the current satellite constellation. ~~Furthermore, the present study~~

shows that the spread of (2) The spread obtained for data assimilation impacts among multiple systems can be used to evaluate whether the across multiple systems, including notable differences in certain areas, provide key insights for determining the influence of reanalysis system choices on the observing system impacts are dependent on the reanalysis system. These impact assessments. The absolute values of DA increments largely varied, ranging 0–21%, 0–22%, and 0.1–19% in the UTLS, middle, and lower troposphere, respectively. However, the remaining biases of reanalyses against ozonesonde observations were within $\pm 2.5\%$, $\pm 3.5\%$, and $\pm 7.0\%$ in the UTLS, middle, and lower troposphere, respectively, except for GEOS-Chem adjoint. These differences could be related to a variety of factors, including different retrieval algorithms, data assimilation settings, which are applied to fully exploit observational information (e.g., assumption of background error covariance), and different model performance. These findings should lead to more robust assessments of the observing system impacts. The impact of assimilating OMI tropospheric NO₂ on lower tropospheric ozone varied from +0.1% to +7%. These results indicate that the assessment of observing system impacts is sensitive to the choice of data assimilation system. This difference reflects a variety of factors, including may reflect the different a priori surface NO_x emissions between TCR-2 (46.48 Tg N yr⁻¹) and GEOS-Chem (52.20 Tg N yr⁻¹) (Table S1) as well as differing model resolutions (Sekiya et al., 2021). Additionally, systematic biases among the assimilated products derived from different retrieval algorithms (Qu et al., 2020), inappropriate data assimilation settings to fully exploit observational information (e.g., underestimation of background errors), and different model biases among systems may contribute to these differences (Qu et al., 2020). GEOS-Chem adjoint shows larger data assimilation impacts on ozone when assimilating the DOMINO product than the NASA standard product (Figure S2).

However, even with improved observing systems, the impact of data assimilation will be limited because of the different complexities of chemical mechanisms (Huijnen et al., 2019; Miyazaki et al., 2020b), deposition processes (Hardacre et al., 2015; Young et al., 2018), and model physics, such as cloud formation and convective transport. Furthermore, VOCs such as formaldehyde (De Smedt et al., 2018) and isoprene (Wells et al., 2022) have not commonly been assimilated in the current chemical reanalysis systems. The lack of observations on important factors that determine chemical ozone formation underscores the need to fully exploit available observational information and causes underestimates of the value of the current observational system in the reanalysis framework.

Current chemical reanalysis systems employ various data assimilation techniques, including 3D-Var, 4D-Var, and EnKF. These approaches differ in their assumptions and concepts and therefore in their performance (Lorenc and Rawlins, 2005; Kalnay et al., 2007). 4D-Var and EnKF exhibit comparable performance for both meteorological (Miyoshi et al., 2010) and chemical data assimilation (Wu et al., 2008; Skachko et al., 2014). A specific challenge in chemical data assimilation that differs from NWP is that chemical systems are stiff, stable non-chaotic, and highly dependent on input parameters, such as emissions and kinetic parameters (Carmichael et al., 2008; Miyazaki et al., 2012a). Therefore, the optimization of precursor emissions is considered as an essential component of ozone analysis and OSE to provide a more meaningful evaluation of the current observing system. The feasibility and performance of emissions optimization using satellite observations, which have limited sensitivity to the lower troposphere, depends on data assimilation approaches. Nevertheless, optimizing precursor emissions using either online (i.e., simultaneous optimization of concentrations and emissions of various species) or offline

(e.g., independent mass balance of a single species) approaches is important for improving the performance of OSE and reanalysis.

510 The OSEs presented in this study have important implications for improving the integration of future observations, including geostationary orbit (GEO) satellites and surface observations, in addition to low Earth orbit (LEO) satellites. The current satellite observing system provides unique and essential information that are essential for improving ozone analysis throughout the troposphere and stratosphere, as demonstrated in this study. However, the termination or retirement of current instruments such as OMI, MLS, MOPITT, and IASI in the near future may impact the ability to constrain whole troposphere
515 ozone profiles effectively. More recent and future satellite measurements, such as TROPOMI, CrIS, and IASI-New Generation (NG) offer the potential to maintain or even improve constraints on tropospheric ozone and its precursors. For instance, advances in TROPOMI NO₂ assimilation compared to OMI NO₂ assimilation, as demonstrated by Sekiya et al. (2022), highlight these capabilities. For UTLS ozone analysis, several measurements, such as OMPS and SAGE III, continue to provide valuable profile measurements. Nevertheless, the uniqueness of MLS to observe through clouds and aerosols and a wide
520 range of trace gases remains powerful in constraining tropospheric ozone profiles and chemistry system. The development of follow-on missions, such as the Atmospheric Limb Tracker for Investigation of the Upcoming Stratosphere (ALTIUS) (Fussen et al., 2019) and the Stratosphere Troposphere Response using Infrared Vertically-Resolved Light Explorer (STRIVE), to fill the gaps is highly desirable for maintaining high-quality tropospheric ozone analysis. Assessing the observational impacts of these instruments through data assimilation is expected to provide critical information for optimizing the observation system.
525 The multi-system analysis suggested that the model bias at the surface is hardly reduced by the assimilation of any satellites. This highlights the importance of the data assimilation in surface observations (Kong et al., 2021) and machine learning (ML)-based bias corrections (He et al., 2022). However, obtaining sufficient global coverage for surface observing system remains a challenge. The simultaneous assimilation of LEO and GEO satellites, such as GEMS, TEMPO, and Sentinel-4, is expected to improve our understanding of nonlinear ozone chemistry and its diurnal cycles at the urban scale across different regions.
530 Moreover, such assimilation will allow us to estimate uncertain model parameters, such as diurnal emission profiles, kinetic reactions, and photolysis rates (Zoogman et al., 2014; Timmermans et al., 2019; Quesada-Ruiz et al., 2020; Shu et al., 2023). Advanced data assimilation techniques such as 4D-Var and EnKF are required to simultaneously and effectively assimilate observations from different platforms.

6 Summary and conclusion

535 The IGAC TOAR-II Chemical Reanalysis WG activities ~~summarized~~ summarize the capabilities of current chemical reanalysis products for various scientific applications. In this study, we evaluated the relative impacts of ~~the~~ assimilating satellite measurements of ozone and its precursors on surface and free tropospheric ozone analysis using five global chemical reanalysis systems, namely, CAMSRA, TCR-2, IASI-r, GEOS-Chem, and RAQMS, for 2010. The use of multiple reanalysis systems allows for observing system impact assessments that are less dependent on the performance of individual forecast
540 models and the configurations of individual data assimilation systems. Without data assimilation, large standard deviations

in the ozone concentrations between the different models were found in the control runs. For example, the standard deviations were 27%, 8%, and 9% for UTLS, middle troposphere, and lower troposphere, respectively. Data assimilation improved the inter-system agreement and reduced the standard deviation to 3.2%, 1.7%, and 2.5% for UTLS, middle troposphere, and lower troposphere, respectively. In most cases, the consistency with independent ozonesonde observations was also improved by data assimilation. ~~The After data assimilation, the~~ RMSEs against global ozonesonde observations were reduced from ~~27 to 56%~~ to 30% in the UTLS, from 28% to 23% in the middle troposphere, and ~~lower troposphere to 23 to 30% by data assimilation~~ from 27% to 24% in the lower troposphere. However, biases against surface in situ observations showed limited improvements after data assimilation in any of the reanalysis systems. This finding ~~was probably because of the common positive biases of surface ozone in global models (e.g., Turnock et al., 2020) and the low sensitivity of satellite observations to surface ozone~~ is likely related to the limited sensitivity of satellite observations in directly constraining surface ozone. This suggests that reanalysis surface ozone biases may be largely influenced by biases in the forecast models, such as the widely recognized positive bias over major polluted regions reported in various CTM and chemistry-climate model (CCM) simulation (Travis et al., 2016; Young et al., 2018; Turnock et al., 2020). Similar to CTMs and CCMs, the forecast models used in chemical reanalyses incorporate varying degrees of complexity in their chemical mechanisms. The maturity of these forecast models, including effective optimization applied specifically for surface ozone, may have contributed to the smaller surface ozone biases observed in CAMSRA and RAQMS.

Although the assimilated observations varied among the reanalysis systems, we examined the relative impacts of satellite ozone and precursor measurements and their dependence on reanalysis systems with additional OSEs in similar settings across some of the systems. These OSEs suggested the importance of including precursor measurements, especially for NO_x, to improve ozone analysis ~~for in~~ the middle and lower troposphere over the northern midlatitudes, which led to reductions of 58–92% in model ozone biases relative to ozonesonde observations. In addition, the impact of these measurements varied widely between the systems, ranging from +0.1% (GEOS-Chem) to +7% (TCR-2), reflecting model settings and assimilated satellite products. The impacts of direct ozone assimilation showed qualitatively similar latitudinal and vertical patterns between IASI-r and TCR-2, with increases by 6–22% and decreases by 2–21% in the middle troposphere and UTLS, respectively. The consistency with the ozonesonde observations was improved by the assimilation of ozone and its precursors, with bias reductions of up to 68% over the tropical middle troposphere and up to 89% over the middle troposphere over the northern mid-latitudes, respectively. The impacts of direct ozone assimilation were dominant for the UTLS, with bias reductions of up to 91±9% over the northern mid-latitudes.

In conclusion, the simultaneous assimilation of satellite measurements of stratospheric and tropospheric ozone, and its precursors ~~is an effective way to improve the overall~~ has proven to be an effective approach for improving the entire tropospheric ozone analysis. ~~The UTLS and middle tropospheric ozone analyses were consistently improved by satellite observations of the stratospheric and tropospheric ozone profiles, and the middle and lower tropospheric ozone analyses were also improved by the satellite observations of the~~ Despite variations in forecast model performance, assimilated observations, and data assimilation settings across the reanalysis systems used in the intercomparison, data assimilation greatly improved consistency among reanalysis products as well as with independent observations. The overall good agreement suggests that the highly accurate

reanalysis datasets are valuable for advancing our understanding of atmospheric composition variations and can also inform discussions on the development of observing systems. Meanwhile, multi-system OSEs qualitatively demonstrated that ozone analyses from the middle troposphere to the lower stratosphere are improved through the assimilation of satellite ozone observations, while analyses from the lower to middle troposphere benefit from the assimilation of ozone precursors. ~~The impacts of assimilating~~ However, the impacts of ozone assimilation from satellite observations on ozone analysis ~~varied widely among the different reanalysis systems. Further investigation of the model dependence of the assimilating ozone precursor observations with more reanalysis systems is required to assess the uncertainties in the background error covariance between concentrations and emissions. These results indicate the importance of considering the effects of the~~ varies widely across the reanalysis systems, suggesting that individual results may introduce biases when evaluating the value of specific observing systems. This underscores the importance of employing multiple systems to ensure robustness in assessing individual observing systems. Furthermore, these findings highlight the need to account for the forecast model performance and data assimilation configurations ~~on the~~ when conducting OSEs/OSSEs. Such considerations, which have been lacking in previous observing system impact assessments ~~in order to provide an unbiased basis for the discussion of future observing system designs,~~ are essential to provide unbiased insights for designing future observing systems. Meanwhile, to draw more robust conclusions ~~about the system dependence of observing system impact assessments, further studies involving intercomparisons of OSEs conducted with a more consistent and improved protocol compared to the present study are needed.~~

Data availability. CAMS data are freely available from <https://atmosphere.copernicus.eu/data>. TCR-2 data can publicly be accessed at <https://disc.gsfc.nasa.gov/information/data-release?title=Release%20of%20TROPESS%20Chemical%20Reanalysis%20Products>. RAQMS chemical reanalysis data are archived at the University of Wisconsin-Madison Space Science and Engineering Center (SSEC) and can be made available upon request to R. B. Pierce. IASI-r data can be publicly accessed at <https://b2share.cerfacs.fr/records/e3493962fb0e4e6b918d846b070de9d9>. GEOS-Chem-adjoint top-down NO_x emission data are available at <https://dataverse.harvard.edu/dataset.xhtml?persistentId=doi:10.7910/DVN/HVT1FO>.

Author contributions. K.M., D.J., and H.W. designed the research. T.S., E.E., and W.C. performed the analysis. E.E., K.M., A.I., Z.Q., and B.P. provided chemical reanalysis products and OSE results. All the authors wrote and edited the paper manuscript.

600 *Competing interests.* The contact author has declared that neither they nor their co-authors have any competing interests.

Acknowledgements. The Copernicus Atmosphere Monitoring Service is operated by the European Centre for Medium-Range Weather Forecasts (ECMWF) on behalf of the European Commission as part of the Copernicus Programme (<http://copernicus.eu>). The TCR-2 product was generated by the calculations using the Earth Simulator with the support of the Japan Agency for Marine-Earth Science and Technol-

ogy. Part of this work was conducted at the Jet Propulsion Laboratory, California Institute of Technology, under contract with the NASA.
605 The RAQMS chemical reanalysis was supported by funding from the NASA Aura and Health and Air Quality (HAQ) Science Teams. We acknowledge the support of the National Aeronautics and Space Administration (NASA) Atmospheric Composition: Aura Science Team Program (19-AURAST19-0044), Atmospheric Composition Modeling and Analysis Program (22-ACMAP22-0013), NASA Earth Science U.S. Participating Investigator program (22-EUSPI22-0005). This work was also supported by the Environment Research and Technology Development Fund (JPMEERF20222001) of the Ministry of Environment of Japan and the JSPS KAKENHI grants (22K12353, 23H04971).

610 References

- Aabaribaoune, M. E., Emili, E., and Guidard, V.: Estimation of the error covariance matrix for IASI radiances and its impact on the assimilation of ozone in a chemistry transport model, *Atmospheric Measurement Techniques*, 14, 2841–2856, <https://doi.org/10.5194/amt-14-2841-2021>, 2021.
- August, T., Klaes, D., Schlüssel, P., Hultberg, T., Crapeau, M., Arriaga, A., O’Carroll, A., Coppens, D., Munro, R., and Calbet, X.: IASI on Metop-A: Operational Level 2 retrievals after five years in orbit, *J. Quant. Spectrosc. Radiat. Transf.*, 113, 1340–1371, <https://doi.org/10.1016/j.jqsrt.2012.02.028>, 2012.
- 615 Barré, J., Gaubert, B., Arellano, A. F. J., Worden, H. M., Edwards, D. P., Deeter, M. N., Anderson, J. L., Raeder, K., Collins, N., Tilmes, S., Francis, G., Clerbaux, C., Emmons, L. K., Pfister, G. G., Coheur, P.-F., and Hurtmans, D.: Assessing the impacts of assimilating IASI and MOPITT CO retrievals using CESM-CAM-chem and DART, *J. Geophys. Res.*, 120, 10,501–10,529, <https://doi.org/10.1002/2015JD023467>, 2015.
- 620 Beer, R.: TES on the aura mission: scientific objectives, measurements, and analysis overview, *IEEE Trans. Geosci. Remote Sens.*, 44, 1102–1105, <https://doi.org/10.1109/TGRS.2005.863716>, 2006.
- Boersma, K. F., Eskes, H. J., Veefkind, J. P., Brinkma, E. J., van der A, R. J., Sneep, M., van den Oord, G. H. J., Levelt, P. F., Stammes, P., Gleason, J. F., and Bucsela, E. J.: Near-real time retrieval of tropospheric NO₂ from OMI, *Atmos. Chem. Phys.*, 7, 2103–2118, <https://doi.org/10.5194/acp-7-2103-2007>, 2007.
- 625 Boersma, K. F., Eskes, H., Richter, A., De Smedt, I., Lorente, A., Beirle, S., Van Geffen, J., Peters, E., Van Roozendaal, M., and Wagner, T.: QA4ECV NO₂ tropospheric and stratospheric vertical column data from OMI (Version 1.1) [Data set], <https://doi.org/10.21944/qa4ecv-no2-omi-v1.1>, Royal Netherlands Meteorological Institute (KNMI), 2017a.
- Boersma, K. F., Eskes, H., Richter, A., De Smedt, I., Lorente, A., Beirle, S., Van Geffen, J., Peters, E., Van Roozendaal, M., and Wagner, T.: QA4ECV NO₂ tropospheric and stratospheric vertical column data from GOME-2A (Version 1.1) [Data set], <https://doi.org/10.21944/qa4ecv-no2-gome2a-v1.1>, Royal Netherlands Meteorological Institute (KNMI), 2017b.
- 630 Boersma, K. F., Eskes, H., Richter, A., De Smedt, I., Lorente, A., Beirle, S., Van Geffen, J., Peters, E., Van Roozendaal, M., and Wagner, T.: QA4ECV NO₂ tropospheric and stratospheric vertical column data from SCIAMACHY (Version 1.1) [Data set], <https://doi.org/10.21944/qa4ecv-no2-sciamachy-v1.1>, Royal Netherlands Meteorological Institute (KNMI), 2017c.
- 635 Boxe, C. S., Worden, J. R., Bowman, K. W., Kulawik, S. S., Neu, J. L., Ford, W. C., Osterman, G. B., Herman, R. L., Eldering, A., Tarasick, D. W., Thompson, A. M., Doughty, D. C., Hoffmann, M. R., and Oltmans, S. J.: Validation of northern latitude Tropospheric Emission Spectrometer stare ozone profiles with ARC-IONS sondes during ARCTAS: sensitivity, bias and error analysis, *Atmos. Chem. Phys.*, 10, 9901–9914, <https://doi.org/10.5194/acp-10-9901-2010>, 2010.
- Bruckner, M., Pierce, R. B., and Lenzen, A.: Examining ENSO-related variability in tropical tropospheric ozone in the RAQMS-Aura chemical reanalysis, *Atmos. Chem. Phys.*, 24, 10 921–10 945, <https://doi.org/10.5194/acp-24-10921-2024>, 2024.
- 640 Burrows, J. P., Weber, M., Buchwitz, M., Rozanov, V., Ladstätter-Weissenmayer, A., Richter, A., DeBeek, R., Hoogen, R., Bramstedt, K., Eichmann, K.-U., Eisinger, M., and Perner, D.: The Global Ozone Monitoring Experiment (GOME): Mission Concept and First Scientific Results, *J. Atmos. Sci.*, 56, 151–175, [https://doi.org/10.1175/1520-0469\(1999\)056<0151:TGOMEG>2.0.CO;2](https://doi.org/10.1175/1520-0469(1999)056<0151:TGOMEG>2.0.CO;2), 1999.
- Byrd, R. H., Lu, P., Nocedal, J., and Zhu, C.: A Limited Memory Algorithm for Bound Constrained Optimization, *SIAM J. Sci. Comput.*, 645 16, 1190–1208, <https://doi.org/10.1137/0916069>, 1995.

- Callies, J., Corpaccioli, E., Eisinger, M., Hahne, A., and Lefebvre, A.: GOME-2- MetOp's second-generation sensor for operational ozone monitoring, *ESA bulletin*, 102, 28–36, 2000.
- Cariolle, D. and Déqué, M.: Southern hemisphere medium-scale waves and total ozone disturbances in a spectral general circulation model, *J. Geophys. Res.*, 91, 10 825–10 846, <https://doi.org/10.1029/JD091iD10p10825>, 1986.
- 650 Cariolle, D. and Teyssède, H.: A revised linear ozone photochemistry parameterization for use in transport and general circulation models: multi-annual simulations, *Atmos. Chem. Phys.*, 7, 2183–2196, <https://doi.org/10.5194/acp-7-2183-2007>, 2007.
- Carmichael, G. R., Sandu, A., Chai, T., Daescu, D. N., Constantinescu, E. M., and Tang, Y.: Predicting air quality: Improvements through advanced methods to integrate models and measurements, *J. Comput. Phys.*, 227, 3540–3571, <https://doi.org/10.1016/j.jcp.2007.02.024>, 2008.
- 655 Chang, K.-L., Cooper, O. R., Gaudel, A., Petropavlovskikh, I., Effertz, P., Morris, G., and McDonald, B. C.: Technical note: Challenges in detecting free tropospheric ozone trends in a sparsely sampled environment, *Atmos. Chem. Phys.*, 24, 6197–6218, <https://doi.org/10.5194/acp-24-6197-2024>, 2024.
- Courtier, P., Thépaut, J.-N., and Hollingsworth, A.: A strategy for operational implementation of 4D-Var, using an incremental approach, *Q. J. R. Meteorol. Soc.*, 120, 1367–1387, <https://doi.org/10.1002/qj.49712051912>, 1994.
- 660 De Smedt, I., Theys, N., Yu, H., Danckaert, T., Lerot, C., Compernelle, S., Van Roozendael, M., Richter, A., Hilboll, A., Peters, E., Pedergnana, M., Loyola, D., Beirle, S., Wagner, T., Eskes, H., van Geffen, J., Boersma, K. F., and Veefkind, P.: Algorithm theoretical baseline for formaldehyde retrievals from S5P TROPOMI and from the QA4ECV project, *Atmos. Meas. Tech.*, 11, 2395–2426, <https://doi.org/10.5194/amt-11-2395-2018>, 2018.
- Dee, D. P., Uppala, S. M., Simmons, A. J., Berrisford, P., Poli, P., Kobayashi, S., Andrae, U., Balmaseda, M. A., Balsamo, G., Bauer, P., 665 Bechtold, P., Beljaars, A. C. M., van de Berg, L., Bidlot, J., Bormann, N., Delsol, C., Dragani, R., Fuentes, M., Geer, A. J., Haimberger, L., Healy, S. B., Hersbach, H., Hólm, E. V., Isaksen, I., Kållberg, P., Köhler, M., Matricardi, M., McNally, A. P., Monge-Sanz, B. M., Morcrette, J.-J., Park, B.-K., Peubey, C., de Rosnay, P., Tavolato, C., Thépaut, J.-N., and Vitart, F.: The ERA-Interim reanalysis: configuration and performance of the data assimilation system, *Q. J. R. Meteorol. Soc.*, 137, 553–597, <https://doi.org/10.1002/qj.828>, 2011.
- Deeter, M. N., Edwards, D. P., Francis, G. L., Gille, J. C., Martínez-Alonso, S., Worden, H. M., and Sweeney, C.: A climate-scale satellite 670 record for carbon monoxide: the MOPITT Version 7 product, *Atmos. Meas. Tech.*, 10, 2533–2555, <https://doi.org/10.5194/amt-10-2533-2017>, 2017.
- Drummond, J. R., Zou, J., Nichitiu, F., Kar, J., Deschambaut, R., and Hackett, J.: A review of 9-year performance and operation of the MOPITT instrument, *Adv. Space Res.*, 45, 760–774, <https://doi.org/10.1016/j.asr.2009.11.019>, 2010.
- Dufour, G., Eremenko, M., Griesfeller, A., Barret, B., LeFlochmoën, E., Clerbaux, C., Hadji-Lazaro, J., Coheur, P.-F., and Hurtmans, D.: 675 Validation of three different scientific ozone products retrieved from IASI spectra using ozonesondes, *Atmos. Meas. Tech.*, 5, 611–630, <https://doi.org/10.5194/amt-5-611-2012>, 2012.
- East, J. D., Henderson, B. H., Napelenok, S. L., Koplitz, S. N., Sarwar, G., Gilliam, R., Lenzen, A., Tong, D. Q., Pierce, R. B., and Garcia-Menendez, F.: Inferring and evaluating satellite-based constraints on NO_x emissions estimates in air quality simulations, *Atmos. Chem. Phys.*, 22, 15 981–16 001, <https://doi.org/10.5194/acp-22-15981-2022>, 2022.
- 680 Elshorbany, Y., Ziemke, J. R., Strode, S., Petetin, H., Miyazaki, K., De Smedt, I., Pickering, K., Seguel, R. J., Worden, H., Emmerichs, T., Taraborrelli, D., Cazorla, M., Fadnavis, S., Buchholz, R. R., Gaubert, B., Rojas, N. Y., Nogueira, T., Salameh, T., and Huang, M.: Tropospheric ozone precursors: global and regional distributions, trends, and variability, *Atmos. Chem. Phys.*, 24, 12 225–12 257, <https://doi.org/10.5194/acp-24-12225-2024>, 2024.

- Emili, E. and El Aabaribaoune, M.: Impact of Infrared Atmospheric Sounding Interferometer (IASI) thermal infrared measurements on
685 global ozone reanalyses, *Geosci. Model Dev.*, 14, 6291–6308, <https://doi.org/10.5194/gmd-14-6291-2021>, 2021.
- Emili, E., Barret, B., Massart, S., Flochmoen, E. L., a Piacentini, Amraoui, L. E., Pannekoucke, O., and Cariolle, D.: Combined assimilation
of IASI and MLS observations to constrain tropospheric and stratospheric ozone in a global chemical transport model, *Atmospheric
Chemistry and Physics*, 14, 177–198, <https://doi.org/10.5194/acp-14-177-2014>, 2014.
- Emili, E., Barret, B., Flochmoen, E. L., and Cariolle, D.: Comparison between the assimilation of IASI Level 2 ozone retrievals and Level
690 1 radiances in a chemical transport model, *Atmospheric Measurement Techniques*, 12, 3963–3984, <https://doi.org/10.5194/amt-12-3963-2019>, 2019.
- Evensen, G.: The ensemble Kalman filter for combined state and parameter estimation, *IEEE Control Syst. Mag.*, 29, 83–104, 2009.
- Fleming, Z. L., Doherty, R. M., von Schneidmesser, E., Malley, C. S., Cooper, O. R., Pinto, J. P., Colette, A., Xu, X., Simpson, D., Schultz,
M. G., Lefohn, A. S., Hamad, S., Moolla, R., Solberg, S., and Feng, Z.: Tropospheric Ozone Assessment Report: Present-day ozone
695 distribution and trends relevant to human health, *Elem. Sci. Anth.*, 6, 12, <https://doi.org/10.1525/elementa.273>, 2018.
- Flemming, J., Huijnen, V., Arteta, J., Bechtold, P., Beljaars, A., Blechschmidt, A.-M., Diamantakis, M., Engelen, R. J., Gaudel, A., Inness,
A., Jones, L., Josse, B., Katragkou, E., Marecal, V., Peuch, V.-H., Richter, A., Schultz, M. G., Stein, O., and Tsikerdekis, A.: Tropospheric
chemistry in the Integrated Forecasting System of ECMWF, *Geosci. Model Dev.*, 8, 975–1003, <https://doi.org/10.5194/gmd-8-975-2015>,
2015.
- 700 Flemming, J., Benedetti, A., Inness, A., Engelen, R. J., Jones, L., Huijnen, V., Remy, S., Parrington, M., Suttie, M., Bozzo, A., Peuch, V.-H.,
Akritidis, D., and Katragkou, E.: The CAMS interim Reanalysis of Carbon Monoxide, Ozone and Aerosol for 2003–2015, *Atmos. Chem.
Phys.*, 17, 1945–1983, <https://doi.org/10.5194/acp-17-1945-2017>, 2017.
- Froidevaux, L., Jiang, Y. B., Lambert, A., Livesey, N. J., Read, W. G., Waters, J. W., Browell, E. V., and coauthors: Validation of Aura
Microwave Limb Sounder Stratospheric Ozone Measurements, *J. Geophys. Res.*, 113, <https://doi.org/10.1029/2007JD008771>, 2008.
- 705 Fussen, D., Baker, N., Deboscher, J., Dekemper, E., Demoulin, P., Errera, Q., Franssens, G., Matshvili, N., Pereira, N., Pier-
oux, D., and Vanhellemont, F.: The ALTIUS atmospheric limb sounder, *J. Quantitative Spectr. Rad. Transf.*, 238, 106 542,
<https://doi.org/10.1016/j.jqsrt.2019.06.021>, 2019.
- Gaubert, B., Arellano Jr., A. F., Barré, J., Worden, H. M., Emmons, L. K., Tilmes, S., Buchholz, R. R., Vitt, F., Raeder, K., Collins, N.,
Anderson, J. L., Wiedinmyer, C., Martinez Alonso, S., Edwards, D. P., Andreae, M. O., Hannigan, J. W., Petri, C., Strong, K., and Jones,
710 N.: Toward a chemical reanalysis in a coupled chemistry-climate model: An evaluation of MOPITT CO assimilation and its impact on
tropospheric composition, *J. Geophys. Res.*, 121, 7310–7343, <https://doi.org/10.1002/2016JD024863>, 2016.
- Gaudel, A., Cooper, O. R., Ancellet, G., Barret, B., Boynard, A., Burrows, J. P., Clerbaux, C., Coheur, P.-F., Cuesta, J., Cuevas, E., Doniki,
S., Dufour, G., Ebojie, F., Foret, G., Garcia, O., Granados-Muñoz, M. J., Hannigan, J. W., Hase, F., Hassler, B., Huang, G., Hurtmans, D.,
Jaffe, D., Jones, N., Kalabokas, P., Kerridge, B., Kulawik, S., Latter, B., Leblanc, T., Le Flochmoen, E., Lin, W., Liu, J., Liu, X., Mahieu,
715 E., McClure-Begley, A., Neu, J. L., Osman, M., Palm, M., Petetin, H., Petropavlovskikh, I., Querel, R., Rahpoe, N., Rozanov, A., Schultz,
M. G., Schwab, J., Siddans, R., Smale, D., Steinbacher, M., Tanimoto, H., Tarasick, D. W., Thouret, V., Thompson, A. M., Trickl, T.,
Weatherhead, E., Wespes, C., Worden, H. M., Vigouroux, C., Xu, X., Zeng, G., and Ziemke, J.: Tropospheric Ozone Assessment Report:
Present-day distribution and trends of tropospheric ozone relevant to climate and global atmospheric chemistry model evaluation, *Elem.
Sci. Anth.*, 6, 39, <https://doi.org/10.1525/elementa.291>, 2018.
- 720 Gaudel, A., Bourgeois, I., Li, M., Chang, K.-L., Ziemke, J., Sauvage, B., Stauffer, R. M., Thompson, A. M., Kollonige, D. E., Smith, N.,
Hubert, D., Keppens, A., Cuesta, J., Heue, K.-P., Veefkind, P., Aikin, K., Peischl, J., Thompson, C. R., Ryerson, T. B., Frost, G. J.,

- McDonald, B. C., and Cooper, O. R.: Tropical tropospheric ozone distribution and trends from in situ and satellite data, *EGUsphere*, 2024, 1–51, <https://doi.org/10.5194/egusphere-2023-3095>, 2024.
- Giglio, L., Randerson, J. T., and van der Werf, G. R.: Analysis of daily, monthly, and annual burned area using the fourth-generation global fire emissions database (GFED4), *J. Geophys. Res.*, 118, 317–328, <https://doi.org/10.1002/jgrg.20042>, 2013.
- 725 Graedel, T. E., Bates, T. S., Bouwman, A. F., Cunnold, D., Dignon, J., Fung, I., Jacob, D. J., Lamb, B. K., Logan, J. A., Marland, G., Middleton, P., Pacyna, J. M., Placet, M., and Veldt, C.: A compilation of inventories of emissions to the atmosphere, *Global Biogeochem. Cy.*, 7, 1–26, <https://doi.org/10.1029/92GB02793>, 1993.
- Granier, C., Bessagnet, B., Bond, T., D’Angiola, A., Denier van der Gon, H., Frost, G. J., Heil, A., Kaiser, J. W., Kinne, S., Klimont, Z., Kloster, S., Lamarque, J.-F., Liousse, C., Masui, T., Meleux, F., Mieville, A., Ohara, T., Raut, J.-C., Riahi, K., Schultz, M. G., Smith, S. J., Thompson, A., van Aardenne, J., van der Werf, G. R., and van Vuuren, D. P.: Evolution of anthropogenic and biomass burning emissions of air pollutants at global and regional scales during the 1980–2010 period, *Clim. Change*, 109, 163, <https://doi.org/10.1007/s10584-011-0154-1>, 2011.
- 730 Hanea, R. G., Velders, G. J. M., and Heemink, A.: Data assimilation of ground-level ozone in Europe with a Kalman filter and chemistry transport model, *J. Geophys. Res.*, 109, <https://doi.org/10.1029/2003JD004283>, 2004.
- Hardacre, C., Wild, O., and Emberson, L.: An evaluation of ozone dry deposition in global scale chemistry climate models, *Atmos. Chem. Phys.*, 15, 6419–6436, <https://doi.org/10.5194/acp-15-6419-2015>, 2015.
- He, T.-L., Jones, D. B. A., Miyazaki, K., Huang, B., Liu, Y., Jiang, Z., White, E. C., Worden, H. M., and Worden, J. R.: Deep Learning to Evaluate US NO_x Emissions Using Surface Ozone Predictions, *J. Geophys. Res.*, 127, e2021JD035597, <https://doi.org/10.1029/2021JD035597>, 2022.
- 740 Henze, D. K., Hakami, A., and Seinfeld, J. H.: Development of the adjoint of GEOS-Chem, *Atmos. Chem. Phys.*, 7, 2413–2433, <https://doi.org/10.5194/acp-7-2413-2007>, 2007.
- Huang, M., Carmichael, G. R., Chai, T., Pierce, R. B., Oltmans, S. J., Jaffe, D. A., Bowman, K. W., Kaduwela, A., Cai, C., Spak, S. N., Weinheimer, A. J., Huey, L. G., and Diskin, G. S.: Impacts of transported background pollutants on summertime western US air quality: model evaluation, sensitivity analysis and data assimilation, *Atmos. Chem. Phys.*, 13, 359–391, <https://doi.org/10.5194/acp-13-359-2013>, 2013.
- 745 Huijnen, V., Williams, J., van Weele, M., van Noije, T., Krol, M., Dentener, F., Segers, A., Houweling, S., Peters, W., de Laat, J., Boersma, F., Bergamaschi, P., van Velthoven, P., Le Sager, P., Eskes, H., Alkemade, F., Scheele, R., Nédélec, P., and Pätz, H.-W.: The global chemistry transport model TM5: description and evaluation of the tropospheric chemistry version 3.0, *Geosci. Model Dev.*, 3, 445–473, <https://doi.org/10.5194/gmd-3-445-2010>, 2010.
- Huijnen, V., Pozzer, A., Arteta, J., Brasseur, G., Bouarar, I., Chabrillat, S., Christophe, Y., Doumbia, T., Flemming, J., Guth, J., Josse, B., Karydis, V. A., Marécal, V., and Pelletier, S.: Quantifying uncertainties due to chemistry modelling – evaluation of tropospheric composition simulations in the CAMS model (cycle 43R1), *Geosci. Model Dev.*, 12, 1725–1752, <https://doi.org/10.5194/gmd-12-1725-2019>, 2019.
- 750 Huijnen, V., Miyazaki, K., Flemming, J., Inness, A., Sekiya, T., and Schultz, M. G.: An intercomparison of tropospheric ozone reanalysis products from CAMS, CAMS interim, TCR-1, and TCR-2, *Geosci. Model Dev.*, 13, 1513–1544, <https://doi.org/10.5194/gmd-13-1513-2020>, 2020.
- Hunt, B. R., Kostelich, E. J., and Szunyogh, I.: Efficient data assimilation for spatiotemporal chaos: A local ensemble transform Kalman filter, *Physica D*, 230, 112–126, <https://doi.org/10.1016/j.physd.2006.11.008>, 2007.

- 760 Inness, A., Baier, F., Benedetti, A., Bouarar, I., Chabrillat, S., Clark, H., Clerbaux, C., Coheur, P., Engelen, R. J., Errera, Q., Flemming, J., George, M., Granier, C., Hadji-Lazarou, J., Huijnen, V., Hurtmans, D., Jones, L., Kaiser, J. W., Kapsomenakis, J., Lefever, K., Leitão, J., Razinger, M., Richter, A., Schultz, M. G., Simmons, A. J., Suttie, M., Stein, O., Thépaut, J.-N., Thouret, V., Vrekoussis, M., Zerefos, C., and the MACC team: The MACC reanalysis: an 8 yr data set of atmospheric composition, *Atmos. Chem. Phys.*, 13, 4073–4109, <https://doi.org/10.5194/acp-13-4073-2013>, 2013.
- 765 Inness, A., Ades, M., Agustí-Panareda, A., Barré, J., Benedictow, A., Blechschmidt, A.-M., Dominguez, J. J., Engelen, R., Eskes, H., Flemming, J., Huijnen, V., Jones, L., Kipling, Z., Massart, S., Parrington, M., Peuch, V.-H., Razinger, M., Remy, S., Schulz, M., and Suttie, M.: The CAMS reanalysis of atmospheric composition, *Atmos. Chem. Phys.*, 19, 3515–3556, <https://doi.org/10.5194/acp-19-3515-2019>, 2019.
- Inness, A., Aben, I., Ades, M., Borsdorff, T., Flemming, J., Jones, L., Landgraf, J., Langerock, B., Nedelec, P., Parrington, M., and Ribas, R.:
770 Assimilation of S5P/TROPOMI carbon monoxide data with the global CAMS near-real-time system, *Atmos. Chem. Phys.*, 22, 14355–14376, <https://doi.org/10.5194/acp-22-14355-2022>, 2022.
- Janssens-Maenhout, G., Crippa, M., Guizzardi, D., Dentener, F., Muntean, M., Pouliot, G., Keating, T., Zhang, Q., Kurokawa, J., Wankmüller, R., Denier van der Gon, H., Kuenen, J. J. P., Klimont, Z., Frost, G., Darras, S., Koffi, B., and Li, M.: HTAP_v2.2: a mosaic of regional and global emission grid maps for 2008 and 2010 to study hemispheric transport of air pollution, *Atmos. Chem. Phys.*, 15, 11411–11432,
775 <https://doi.org/10.5194/acp-15-11411-2015>, 2015.
- Jin, X., Fiore, A., Boersma, K. F., Smedt, I. D., and Valin, L.: Inferring Changes in Summertime Surface Ozone–NO_x–VOC Chemistry over U.S. Urban Areas from Two Decades of Satellite and Ground-Based Observations, *Environ. Sci. Technol.*, 54, 6518–6529, <https://doi.org/10.1021/acs.est.9b07785>, 2020.
- Josse, B., Simon, P., and Peuch, V.: Radon global simulations with the multiscale chemistry and transport model MOCAGE, *Tellus B*, 56,
780 339–356, <https://doi.org/10.1111/j.1600-0889.2004.00112.x>, 2004.
- Kaiser, J. W., Heil, A., Andreae, M. O., Benedetti, A., Chubarova, N., Jones, L., Morcrette, J.-J., Razinger, M., Schultz, M. G., Suttie, M., and van der Werf, G. R.: Biomass burning emissions estimated with a global fire assimilation system based on observed fire radiative power, *Biogeosciences*, 9, 527–554, <https://doi.org/10.5194/bg-9-527-2012>, 2012.
- Kalnay, E., Li, H., Miyoshi, T., Yang, S.-C., and Ballabrera-Poy, J.: 4-D-Var or ensemble Kalman filter?, *Tellus A: Dyn. Meteorol. Oceanogr.*,
785 59, 758–773, <https://doi.org/10.1111/j.1600-0870.2007.00261.x>, 2007.
- Kleist, D. T., Parrish, D. F., Derber, J. C., Treadon, R., Wu, W.-S., and Lord, S.: Introduction of the GSI into the NCEP Global Data Assimilation System, *Weather and Forecasting*, 24, 1691–1705, <https://doi.org/10.1175/2009WAF2222201.1>, 2009.
- Kong, L., Tang, X., Zhu, J., Wang, Z., Li, J., Wu, H., Wu, Q., Chen, H., Zhu, L., Wang, W., Liu, B., Wang, Q., Chen, D., Pan, Y., Song, T., Li, F., Zheng, H., Jia, G., Lu, M., Wu, L., and Carmichael, G. R.: A 6-year-long (2013–2018) high-resolution air quality reanalysis dataset in
790 China based on the assimilation of surface observations from CNEMC, *Earth Syst. Sci. Data*, 13, 529–570, <https://doi.org/10.5194/essd-13-529-2021>, 2021.
- Krotkov, N. A., Lamsal, L. N., Celarier, E. A., Swartz, W. H., Marchenko, S. V., Bucsela, E. J., Chan, K. L., Wenig, M., and Zara, M.: The version 3 OMI NO₂ standard product, *Atmos. Meas. Tech.*, 10, 3133–3149, <https://doi.org/10.5194/amt-10-3133-2017>, 2017.
- Lahoz, W., Khatatov, B., and Menard, R.: *Data Assimilation: Making Sense of Observations*, Springer Berlin Heidelberg, 2010.
- 795 Lee, H.-J., Chang, L.-S., Jaffe, D. A., Bak, J., Liu, X., Abad, G. G., Jo, H.-Y., Jo, Y.-J., Lee, J.-B., Yang, G.-H., Kim, J.-M., and Kim, C.-H.: Satellite-Based Diagnosis and Numerical Verification of Ozone Formation Regimes over Nine Megacities in East Asia, *Remote Sensing*, 14, <https://doi.org/10.3390/rs14051285>, 2022.

- Levelt, P., van den Oord, G., Dobber, M., Malkki, A., Visser, H., de Vries, J., Stammes, P., Lundell, J., and Saari, H.: The ozone monitoring instrument, *IEEE Trans. Geosci. Remote Sens.*, 44, 1093–1101, <https://doi.org/10.1109/TGRS.2006.872333>, 2006.
- 800 Li, C., Joiner, J., Krotkov, N. A., and Bhartia, P. K.: A fast and sensitive new satellite SO₂ retrieval algorithm based on principal component analysis: Application to the ozone monitoring instrument, *Geophys. Res. Lett.*, 40, 6314–6318, <https://doi.org/10.1002/2013GL058134>, 2013.
- Livesey, N. J., Read, W. G., Wagner, P. A., Froidevaux, L., Lambert, A., Manney, G. L., Millán Valle, L. F., Pumphrey, H. C., Santee, M. L., Schwartz, M. J., Wang, S., Fuller, R. A., Jarnot, R. F., Knosp, B. W., Martinez, E., and Lay, R. R.: Aura Microwave Limb Sounder (MLS) Version 4.2x Level2 data quality and description document, Tech. rep., Jet Propul. Lab., Pasadena, CA, tech. Rep. JPL D33509 Rev. D, 2018.
- 805 Lorenc, A. C. and Rawlins, F.: Why does 4D-Var beat 3D-Var?, *Q. J. R. Meteorol. Soc.*, 131, 3247–3257, <https://doi.org/10.1256/qj.05.85>, 2005.
- McPeters, R., Kroon, M., Labow, G., Brinksma, E., Balis, D., Petropavlovskikh, I., Veefkind, J. P., Bhartia, P. K., and Levelt, P. F.: Validation of the Aura Ozone Monitoring Instrument Total Column Ozone Product, *J. Geophys. Res.*, 113, <https://doi.org/10.1029/2007JD008802>, 2008.
- 810 Mills, G., Pleijel, H., Malley, C. S., Sinha, B., Cooper, O. R., Schultz, M. G., Neufeld, H. S., Simpson, D., Sharps, K., Feng, Z., Gerosa, G., Harmens, H., Kobayashi, K., Saxena, P., Paoletti, E., Sinha, V., and Xu, X.: Tropospheric Ozone Assessment Report: Present-day tropospheric ozone distribution and trends relevant to vegetation, *Elementa: Science of the Anthropocene*, 6, 47, <https://doi.org/10.1525/elementa.302>, 2018.
- Miyazaki, K. and Bowman, K.: Evaluation of ACCMIP ozone simulations and ozonesonde sampling biases using a satellite-based multi-constituent chemical reanalysis, *Atmos. Chem. Phys.*, 17, 8285–8312, <https://doi.org/10.5194/acp-17-8285-2017>, 2017.
- Miyazaki, K., Eskes, H. J., and Sudo, K.: Global NO_x emission estimates derived from an assimilation of OMI tropospheric NO₂ columns, *Atmos. Chem. Phys.*, 12, 2263–2288, <https://doi.org/10.5194/acp-12-2263-2012>, 2012a.
- 820 Miyazaki, K., Eskes, H. J., Sudo, K., Takigawa, M., van Weele, M., and Boersma, K. F.: Simultaneous assimilation of satellite NO₂, O₃, CO, and HNO₃ data for the analysis of tropospheric chemical composition and emissions, *Atmos. Chem. Phys.*, 12, 9545–9579, <https://doi.org/10.5194/acp-12-9545-2012>, 2012b.
- Miyazaki, K., Sekiya, T., Fu, D., Bowman, K. W., Kulawik, S. S., Sudo, K., Walker, T., Kanaya, Y., Takigawa, M., Ogochi, K., Eskes, H., Boersma, K. F., Thompson, A. M., Gaubert, B., Barre, J., and Emmons, L. K.: Balance of Emission and Dynamical Controls on Ozone During the Korea–United States Air Quality Campaign From Multiconstituent Satellite Data Assimilation, *J. Geophys. Res.*, 124, 387–413, <https://doi.org/10.1029/2018JD028912>, 2019.
- 825 Miyazaki, K., Bowman, K., Sekiya, T., Eskes, H., Boersma, F., Worden, H., Livesey, N., Payne, V. H., Sudo, K., Kanaya, Y., Takigawa, M., and Ogochi, K.: Updated tropospheric chemistry reanalysis and emission estimates, TCR-2, for 2005–2018, *Earth Syst. Sci. Data*, 12, 2223–2259, <https://doi.org/10.5194/essd-12-2223-2020>, 2020a.
- 830 Miyazaki, K., Bowman, K. W., Yumimoto, K., Walker, T., and Sudo, K.: Evaluation of a multi-model, multi-constituent assimilation framework for tropospheric chemical reanalysis, *Atmos. Chem. Phys.*, 20, 931–967, <https://doi.org/10.5194/acp-20-931-2020>, 2020b.
- Miyoshi, T., Sato, Y., and Kadowaki, T.: Ensemble Kalman Filter and 4D-Var Intercomparison with the Japanese Operational Global Analysis and Prediction System, *Mon. Weather Rev.*, 138, 2846 – 2866, <https://doi.org/10.1175/2010MWR3209.1>, 2010.

- Naus, S., Domingues, L. G., Krol, M., Luijkx, I. T., Gatti, L. V., Miller, J. B., Gloor, E., Basu, S., Correia, C., Koren, G., Worden, H. M., Flem-
835 ming, J., Pétron, G., and Peters, W.: Sixteen years of MOPITT satellite data strongly constrain Amazon CO fire emissions, *Atmospheric Chemistry and Physics*, 22, 14 735–14 750, <https://doi.org/10.5194/acp-22-14735-2022>, 2022.
- Park, S., Son, S.-W., Jung, M.-I., Park, J., and Park, S. S.: Evaluation of tropospheric ozone reanalyses with independent ozonesonde obser-
vations in East Asia, *Geosci. Lett.*, 7, 12, <https://doi.org/10.1186/s40562-020-00161-9>, 2020.
- Parrington, M., Jones, D. B. A., Bowman, K. W., Thompson, A. M., Tarasick, D. W., Merrill, J., Oltmans, S. J., Leblanc, T., Witte, J. C., and
840 Millet, D. B.: Impact of the assimilation of ozone from the Tropospheric Emission Spectrometer on surface ozone across North America, *Geophys. Res. Lett.*, 36, <https://doi.org/10.1029/2008GL036935>, 2009.
- Parrish, D. F. and Derber, J. C.: The National Meteorological Center’s Spectral Statistical-Interpolation Analysis System, *Mon. Weather Rev.*,
120, 1747 – 1763, [https://doi.org/10.1175/1520-0493\(1992\)120<1747:TNCSS>2.0.CO;2](https://doi.org/10.1175/1520-0493(1992)120<1747:TNCSS>2.0.CO;2), 1992.
- Peiro, H., Emili, E., Cariolle, D., Barret, B., and Flochmoën, E. L.: Multi-year assimilation of IASI and MLS ozone retrievals:
845 variability of tropospheric ozone over the tropics in response to ENSO, *Atmospheric Chemistry and Physics*, 18, 6939–6958,
<https://doi.org/10.5194/acp-18-6939-2018>, 2018.
- Peuch, V.-H., Engelen, R., Rixen, M., Dee, D., Flemming, J., Suttie, M., Ades, M., Agustí-Panareda, A., Ananasso, C., Andersson, E.,
Armstrong, D., Barré, J., Bousserez, N., Dominguez, J. J., Garrigues, S., Inness, A., Jones, L., Kipling, Z., Letertre-Danczak, J., Parrington,
M., Razinger, M., Ribas, R., Vermoote, S., Yang, X., Simmons, A., de Marcilla, J. G., and Thépaut, J.-N.: The Copernicus Atmosphere
850 Monitoring Service: From Research to Operations, *Bull. Am. Meteorol. Soc.*, 103, E2650 – E2668, <https://doi.org/10.1175/BAMS-D-21-0314.1>, 2022.
- Pierce, R. B., Al-Saadi, J., Kittaka, C., Schaack, T., Lenzen, A., Bowman, K., Szykman, J., Soja, A., Ryerson, T., Thompson, A. M., Bhartia,
P., and Morris, G. A.: Impacts of background ozone production on Houston and Dallas, Texas, air quality during the Second Texas Air
Quality Study field mission, *J. Geophys. Res.*, 114, <https://doi.org/10.1029/2008JD011337>, 2009.
- 855 Qu, Z., Henze, D. K., Capps, S. L., Wang, Y., Xu, X., Wang, J., and Keller, M.: Monthly top-down NO_x emissions for China (2005–2012):
A hybrid inversion method and trend analysis, *J. Geophys. Res.*, 122, 4600–4625, <https://doi.org/10.1002/2016JD025852>, 2017.
- Qu, Z., Henze, D. K., Li, C., Theys, N., Wang, Y., Wang, J., Wang, W., Han, J., Shim, C., Dickerson, R. R., and Ren, X.: SO₂ Emission
Estimates Using OMI SO₂ Retrievals for 2005–2017, *J. Geophys. Res.*, 124, 8336–8359, <https://doi.org/10.1029/2019JD030243>, 2019a.
- Qu, Z., Henze, D. K., Theys, N., Wang, J., and Wang, W.: Hybrid Mass Balance/4D-Var Joint Inversion of NO_x and SO₂ Emissions in East
860 Asia, *J. Geophys. Res.*, 124, 8203–8224, <https://doi.org/10.1029/2018JD030240>, 2019b.
- Qu, Z., Henze, D. K., Cooper, O. R., and Neu, J. L.: Impacts of global NO_x inversions on NO₂ and ozone simulations, *Atmos. Chem. Phys.*,
20, 13 109–13 130, <https://doi.org/10.5194/acp-20-13109-2020>, 2020.
- Quesada-Ruiz, S., Attié, J.-L., Lahoz, W. A., Abida, R., Ricaud, P., El Amraoui, L., Zbinden, R., Piacentini, A., Joly, M., Eskes, H.,
Segers, A., Curier, L., de Haan, J., Kujanpää, J., Oude Nijhuis, A. C. P., Tamminen, J., Timmermans, R., and Veefkind, P.: Benefit of
865 ozone observations from Sentinel-5P and future Sentinel-4 missions on tropospheric composition, *Atmos. Meas. Tech.*, 13, 131–152,
<https://doi.org/10.5194/amt-13-131-2020>, 2020.
- Randerson, J., van der Werf, G., Giglio, L., Collatz, G., and Kasibhatla, P.: Global Fire Emissions Database, Version 4.1 (GFEDv4.1),
<https://doi.org/10.3334/ORNDAAC/1293>, ORNL DAAC, Oak Ridge, Tennessee, USA, 2018.
- Remer, L. A., Kaufman, Y. J., Tanré, D., Mattoo, S., Chu, D. A., Martins, J. V., Li, R. R., and coauthors: The MODIS Aerosol Algorithm,
870 Products, and Validation, *J. Atmos. Sci.*, 62, 947–973, <https://doi.org/10.1175/JAS3385.1>, 2005.

- Ren, J., Guo, F., and Xie, S.: Diagnosing ozone–NO_x–VOC sensitivity and revealing causes of ozone increases in China based on 2013–2021 satellite retrievals, *Atmos. Chem. Phys.*, 22, 15 035–15 047, <https://doi.org/10.5194/acp-22-15035-2022>, 2022.
- Ryu, Y.-H. and Min, S.-K.: Long-term evaluation of atmospheric composition reanalyses from CAMS, TCR-2, and MERRA-2 over South Korea: Insights into applications, implications, and limitations, *Atmos. Environ.*, 246, 118 062, <https://doi.org/10.1016/j.atmosenv.2020.118062>, 2021.
- Schaack, T. K., Zapotocny, T. H., Lenzen, A. J., and Johnson, D. R.: Global Climate Simulation with the University of Wisconsin Global Hybrid Isentropic Coordinate Model, *Journal of Climate*, 17, 2998–3016, [https://doi.org/10.1175/1520-0442\(2004\)017<2998:GCSWTU>2.0.CO;2](https://doi.org/10.1175/1520-0442(2004)017<2998:GCSWTU>2.0.CO;2), 2004.
- Schoeberl, M. R., Ziemke, J. R., Bojkov, B., Livesey, N., Duncan, B., Strahan, S., Froidevaux, L., Kulawik, S., Bhartia, P. K., Chandra, S., Levelt, P. F., Witte, J. C., Thompson, A. M., Cuevas, E., Redondas, A., Tarasick, D. W., Davies, J., Bodeker, G., Hansen, G., Johnson, B. J., Oltmans, S. J., Vömel, H., Allaart, M., Kelder, H., Newchurch, M., Godin-Beekmann, S., Ancellet, G., Claude, H., Andersen, S. B., Kyrö, E., Parrondos, M., Yela, M., Zablocki, G., Moore, D., Dier, H., von der Gathen, P., Viatte, P., Stübi, R., Calpini, B., Skrivankova, P., Dorokhov, V., de Backer, H., Schmidlin, F. J., Coetzee, G., Fujiwara, M., Thouret, V., Posny, F., Morris, G., Merrill, J., Leong, C. P., Koenig-Langlo, G., and Joseph, E.: A trajectory-based estimate of the tropospheric ozone column using the residual method, *J. Geophys. Res.*, 112, <https://doi.org/https://doi.org/10.1029/2007JD008773>, 2007.
- Schultz, M. G., Schröder, S., Lyapina, O., Cooper, O. R., Galbally, I., Petropavlovskikh, I., von Schneidemesser, E., Tanimoto, H., Elshorbany, Y., Naja, M., Seguel, R. J., Dauert, U., Eckhardt, P., S., F., Fiebig, M., Hjellbrekke, A.-G., Hong, Y.-D., Kjeld, P. C., Koide, H., Lear, G., Tarasick, D., Ueno, M., Wallasch, M., Baumgardner, D., Chuang, M.-T., Gillett, R., Lee, M., Molloy, S., Moolla, R., Wang, T., Sharps, K., Adame, J. A., Ancellet, G., Apadula, F., Artaxo, P., Barlasina, M. E., Bogucka, M., Bonasoni, P., Chang, L., Colomb, A., Cuevas-Agulló, E., Cupeiro, M., Degorska, A., Ding, A., Fröhlich, M., Frolova, M., Gadhavi, H., Gheusi, F., Gilge, S., Gonzalez, M. Y., Gros, V., Hamad, S. H., Helmig, D., Henriques, D., Hermansen, O., Holla, R., Hueber, J., Im, U., Jaffe, D. A., Komala, N., Kubistin, D., Lam, K.-S., Laurila, T., Lee, H., Levy, I., Mazzoleni, C., Mazzoleni, L. R., McClure-Begley, A., Mohamad, M., Murovec, M., Navarro-Comas, M., Nicodim, F., Parrish, D., Read, K. A., Reid, N., Ries, L., Saxena, P., Schwab, J. J., Scorgie, Y., Senik, I., Simmonds, P., Sinha, V., Skorokhod, A. I., Spain, G., Spangl, W., Spoor, R., Springston, S. R., Steer, K., Steinbacher, M., Suharguniyawan, E., Torre, P., Trickl, T., Weili, L., Weller, R., Xu, X., Xue, L., and Ma, Z.: Tropospheric Ozone Assessment Report, links to Global surface ozone datasets, <https://doi.org/10.1594/PANGAEA.876108>, supplement to: Schultz, MG et al. (2017): Tropospheric Ozone Assessment Report: Database and Metrics Data of Global Surface Ozone Observations. *Elementa - Science of the Anthropocene*, 5:58, 26 pp, <https://doi.org/10.1525/elementa.244>, 2017a.
- Schultz, M. G., Schröder, S., Lyapina, O., Cooper, O. R., Galbally, I., Petropavlovskikh, I., von Schneidemesser, E., Tanimoto, H., Elshorbany, Y., Naja, M., Seguel, R. J., Dauert, U., Eckhardt, P., Feigenspan, S., Fiebig, M., Hjellbrekke, A.-G., Hong, Y.-D., Kjeld, P. C., Koide, H., Lear, G., Tarasick, D., Ueno, M., Wallasch, M., Baumgardner, D., Chuang, M.-T., Gillett, R., Lee, M., Molloy, S., Moolla, R., Wang, T., Sharps, K., Adame, J. A., Ancellet, G., Apadula, F., Artaxo, P., Barlasina, M. E., Bogucka, M., Bonasoni, P., Chang, L., Colomb, A., Cuevas-Agulló, E., Cupeiro, M., Degorska, A., Ding, A., Fröhlich, M., Frolova, M., Gadhavi, H., Gheusi, F., Gilge, S., Gonzalez, M. Y., Gros, V., Hamad, S. H., Helmig, D., Henriques, D., Hermansen, O., Holla, R., Hueber, J., Im, U., Jaffe, D. A., Komala, N., Kubistin, D., Lam, K.-S., Laurila, T., Lee, H., Levy, I., Mazzoleni, C., Mazzoleni, L. R., McClure-Begley, A., Mohamad, M., Murovec, M., Navarro-Comas, M., Nicodim, F., Parrish, D., Read, K. A., Reid, N., Ries, L., Saxena, P., Schwab, J. J., Scorgie, Y., Senik, I., Simmonds, P., Sinha, V., Skorokhod, A. I., Spain, G., Spangl, W., Spoor, R., Springston, S. R., Steer, K., Steinbacher, M., Suharguniyawan, E., Torre, P., Trickl,

- T., Weili, L., Weller, R., Xiaobin, X., Xue, L., and Zhiqiang, M.: Tropospheric Ozone Assessment Report: Database and metrics data of global surface ozone observations, *Elem. Sci. Anth.*, 5, 58, <https://doi.org/10.1525/elementa.244>, 2017b.
- 910 Sekiya, T., Miyazaki, K., Ogochi, K., Sudo, K., and Takigawa, M.: Global high-resolution simulations of tropospheric nitrogen dioxide using CHASER V4.0, *Geosci. Model Dev.*, 11, 959–988, <https://doi.org/10.5194/gmd-11-959-2018>, 2018.
- Sekiya, T., Kanaya, Y., Sudo, K., Taketani, F., Iwamoto, Y., Aita, M. N., Yamamoto, A., and Kawamoto, K.: Global Bromine- and Iodine-Mediated Tropospheric Ozone Loss Estimated Using the CHASER Chemical Transport Model, *SOLA*, 16, 220–227, <https://doi.org/10.2151/sola.2020-037>, 2020.
- 915 Sekiya, T., Miyazaki, K., Ogochi, K., Sudo, K., Takigawa, M., Eskes, H., and Boersma, K. F.: Impacts of Horizontal Resolution on Global Data Assimilation of Satellite Measurements for Tropospheric Chemistry Analysis, *J. Adv. Model. Earth Syst.*, 13, e2020MS002180, <https://doi.org/10.1029/2020MS002180>, 2021.
- Sekiya, T., Miyazaki, K., Eskes, H., Sudo, K., Takigawa, M., and Kanaya, Y.: A comparison of the impact of TROPOMI and OMI tropospheric NO₂ on global chemical data assimilation, *Atmos. Meas. Tech.*, 15, 1703–1728, <https://doi.org/10.5194/amt-15-1703-2022>, 2022.
- 920 Sherwen, T., Schmidt, J. A., Evans, M. J., Carpenter, L. J., Großmann, K., Eastham, S. D., Jacob, D. J., Dix, B., Koenig, T. K., Sinreich, R., Ortega, I., Volkamer, R., Saiz-Lopez, A., Prados-Roman, C., Mahajan, A. S., and Ordóñez, C.: Global impacts of tropospheric halogens (Cl, Br, I) on oxidants and composition in GEOS-Chem, *Atmos. Chem. Phys.*, 16, 12 239–12 271, <https://doi.org/10.5194/acp-16-12239-2016>, 2016.
- Shu, L., Zhu, L., Bak, J., Zoogman, P., Han, H., Liu, S., Li, X., Sun, S., Li, J., Chen, Y., Pu, D., Zuo, X., Fu, W., Yang, X., and Fu, T.-M.: Improving ozone simulations in Asia via multisource data assimilation: results from an observing system simulation experiment with GEMS geostationary satellite observations, *Atmos. Chem. Phys.*, 23, 3731–3748, <https://doi.org/10.5194/acp-23-3731-2023>, 2023.
- Sindelarova, K., Granier, C., Bouarar, I., Guenther, A., Tilmes, S., Stavroukou, T., Müller, J.-F., Kuhn, U., Stefani, P., and Knorr, W.: Global data set of biogenic VOC emissions calculated by the MEGAN model over the last 30 years, *Atmos. Chem. Phys.*, 14, 9317–9341, <https://doi.org/10.5194/acp-14-9317-2014>, 2014.
- 930 Skachko, S., Errera, Q., Ménard, R., Christophe, Y., and Chabrillat, S.: Comparison of the ensemble Kalman filter and 4D-Var assimilation methods using a stratospheric tracer transport model, *Geosci. Model Dev.*, 7, 1451–1465, <https://doi.org/10.5194/gmd-7-1451-2014>, 2014.
- Smit, H. G. J., Straeter, W., Johnson, B. J., Oltmans, S. J., Davies, J., Tarasick, D. W., Hoegger, B., Stubi, R., Schmidlin, F. J., Northam, T., Thompson, A. M., Witte, J. C., Boyd, I., and Posny, F.: Assessment of the performance of ECC-ozonesondes under quasi-flight conditions in the environmental simulation chamber: Insights from the Juelich Ozone Sonde Intercomparison Experiment (JOSIE), *J. Geophys. Res.*, 112, <https://doi.org/10.1029/2006JD007308>, 2007.
- 935 Soja, A. J., Cofer, W. R., Shugart, H. H., Sukhinin, A. I., Stackhouse Jr., P. W., McRae, D. J., and Conard, S. G.: Estimating fire emissions and disparities in boreal Siberia (1998–2002), *J. Geophys. Res.*, 109, <https://doi.org/10.1029/2004JD004570>, 2004.
- Stein, O., Schultz, M. G., Bouarar, I., Clark, H., Huijnen, V., Gaudel, A., George, M., and Clerbaux, C.: On the wintertime low bias of Northern Hemisphere carbon monoxide found in global model simulations, *Atmos. Chem. Phys.*, 14, 9295–9316, <https://doi.org/10.5194/acp-14-9295-2014>, 2014.
- 940 Szopa, S., Naik, V., Adhikary, B., Artaxo, P., Berntsen, T., Collins, W., Fuzzi, S., Gallardo, L., Kiendler-Scharr, A., Klimont, Z., Liao, H., Unger, N., and Zanis, P.: Short-Lived Climate Forcers, in: *Climate Change 2021: The Physical Science Basis*, edited by Masson-Delmotte, V., Zhai, P., Pirani, A., Connors, S., C. Péan, S. B., Caud, N., Chen, Y., Goldfarb, L., Gomis, M., Huang, M., Leitzell, K., Lonnoy, E., Matthews, J., Maycock, T., Waterfield, T., Yelekçi, O., Yu, R., and Zhou, B., pp. 817–922, Cambridge University Press, Cambridge, United Kingdom and New York, NY, USA, <https://doi.org/10.1017/9781009157896.008>, 2021.

- Tarasick, D., Galbally, I. E., Cooper, O. R., Schultz, M. G., Ancellet, G., Leblanc, T., Wallington, T. J., Ziemke, J., Liu, X., Steinbacher, M., Staehelin, J., Vigouroux, C., Hannigan, J. W., García, O., Foret, G., Zanis, P., Weatherhead, E., Petropavlovskikh, I., Worden, H., Osman, M., Liu, J., Chang, K.-L., Gaudel, A., Lin, M., Granados-Muñoz, M., Thompson, A. M., Oltmans, S. J., Cuesta, J., Dufour, G., Thouret, V., Hassler, B., Trickl, T., and Neu, J. L.: Tropospheric Ozone Assessment Report: Tropospheric ozone from 1877 to 2016, observed levels, trends and uncertainties, *Elem. Sci. Anth.*, 7, 39, <https://doi.org/10.1525/elementa.376>, 2019.
- 950
- Tilmes, S., Lamarque, J.-F., Emmons, L. K., Conley, A., Schultz, M. G., Saunio, M., Thouret, V., Thompson, A. M., Oltmans, S. J., Johnson, B., and Tarasick, D.: Technical Note: Ozonesonde climatology between 1995 and 2011: description, evaluation and applications, *Atmos. Chem. Phys.*, 12, 7475–7497, <https://doi.org/10.5194/acp-12-7475-2012>, 2012.
- Timmermans, R., Segers, A., Curier, L., Abida, R., Attié, J.-L., El Amraoui, L., Eskes, H., de Haan, J., Kujanpää, J., Lahoz, W., Oude Nijhuis, A., Quesada-Ruiz, S., Ricaud, P., Veeffkind, P., and Schaap, M.: Impact of synthetic space-borne NO₂ observations from the Sentinel-4 and Sentinel-5P missions on tropospheric NO₂ analyses, *Atmos. Chem. Phys.*, 19, 12 811–12 833, <https://doi.org/10.5194/acp-19-12811-2019>, 2019.
- 955
- Travis, K. R., Jacob, D. J., Fisher, J. A., Kim, P. S., Marais, E. A., Zhu, L., Yu, K., Miller, C. C., Yantosca, R. M., Sulprizio, M. P., Thompson, A. M., Wennberg, P. O., Crouse, J. D., St. Clair, J. M., Cohen, R. C., Laughner, J. L., Dibb, J. E., Hall, S. R., Ullmann, K., Wolfe, G. M., Pollack, I. B., Peischl, J., Neuman, J. A., and Zhou, X.: Why do models overestimate surface ozone in the Southeast United States?, *Atmos. Chem. Phys.*, 16, 13 561–13 577, <https://doi.org/10.5194/acp-16-13561-2016>, 2016.
- 960
- Turnock, S. T., Allen, R. J., Andrews, M., Bauer, S. E., Deushi, M., Emmons, L., Good, P., Horowitz, L., John, J. G., Michou, M., Nabat, P., Naik, V., Neubauer, D., O'Connor, F. M., Olivie, D., Oshima, N., Schulz, M., Sellar, A., Shim, S., Takemura, T., Tilmes, S., Tsigaridis, K., Wu, T., and Zhang, J.: Historical and future changes in air pollutants from CMIP6 models, *Atmos. Chem. Phys.*, 20, 14 547–14 579, <https://doi.org/10.5194/acp-20-14547-2020>, 2020.
- 965
- Veeffkind, J., Aben, I., McMullan, K., Förster, H., de Vries, J., Otter, G., Claas, J., Eskes, H., de Haan, J., Kleipool, Q., van Weele, M., Hasekamp, O., Hoogeveen, R., Landgraf, J., Snel, R., Tol, P., Ingmann, P., Voors, R., Kruizinga, B., Vink, R., Visser, H., and Levelt, P.: TROPOMI on the ESA Sentinel-5 Precursor: A GMES mission for global observations of the atmospheric composition for climate, air quality and ozone layer applications, *Remote Sens. Environ.*, 120, 70–83, <https://doi.org/10.1016/j.rse.2011.09.027>, 2012.
- 970
- Wagner, A., Bennouna, Y., Blechschmidt, A.-M., Brasseur, G., Chabrillat, S., Christophe, Y., Errera, Q., Eskes, H., Flemming, J., Hansen, K. M., Inness, A., Kapsomenakis, J., Langerock, B., Richter, A., Sudarchikova, N., Thouret, V., and Zerefos, C.: Comprehensive evaluation of the Copernicus Atmosphere Monitoring Service (CAMS) reanalysis against independent observations: Reactive gases, *Elem. Sci. Anth.*, 9, 00 171, <https://doi.org/10.1525/elementa.2020.00171>, 2021.
- Waters, J., Froidevaux, L., Harwood, R., Jarnot, R., Pickett, H., Read, W., Siegel, P., Cofield, R., Filipiak, M., Flower, D., Holden, J., Lau, G., Livesey, N., Manney, G., Pumphrey, H., Santee, M., Wu, D., Cuddy, D., Lay, R., Loo, M., Perun, V., Schwartz, M., Stek, P., Thurstans, R., Boyles, M., Chandra, K., Chavez, M., Chen, G.-S., Chudasama, B., Dodge, R., Fuller, R., Girard, M., Jiang, J., Jiang, Y., Knosp, B., LaBelle, R., Lam, J., Lee, K., Miller, D., Oswald, J., Patel, N., Pukala, D., Quintero, O., Scaff, D., Van Snyder, W., Tope, M., Wagner, P., and Walch, M.: The Earth observing system microwave limb sounder (EOS MLS) on the aura Satellite, *IEEE Trans. Geosci. Remote Sens.*, 44, 1075–1092, <https://doi.org/10.1109/TGRS.2006.873771>, 2006.
- 975
- 980
- Wells, K. C., Millet, D. B., Payne, V. H., Vigouroux, C., Aquino, C. A. B., De Mazière, M., de Gouw, J. A., Graus, M., Kurosu, T., Warneke, C., and Wisthaler, A.: Next-Generation Isoprene Measurements From Space: Detecting Daily Variability at High Resolution, *J. Geophys. Res.*, 127, e2021JD036 181, <https://doi.org/10.1029/2021JD036181>, 2022.

- Wu, L., Mallet, V., Bocquet, M., and Sportisse, B.: A comparison study of data assimilation algorithms for ozone forecasts, *J. Geophys. Res.*, 113, <https://doi.org/10.1029/2008JD009991>, 2008.
- 985 Wu, W.-S., Purser, R., and Parrish, D.: Three-Dimensional Variational Analysis with Spatially Inhomogeneous Covariances, *Monthly Weather Review*, 130, 2905–2916, [https://doi.org/10.1175/1520-0493\(2002\)130<2905:TDVAWS>2.0.CO;2](https://doi.org/10.1175/1520-0493(2002)130<2905:TDVAWS>2.0.CO;2), 2002.
- Yarwood, G., Rao, S., Yocke, M., and Whitten, G.: Updates to the carbon bond chemical mechanism: CB05, Final report to the US EPA, RT-0400675, 8, 13, 2005.
- Young, P. J., Naik, V., Fiore, A. M., Gaudel, A., Guo, J., Lin, M. Y., Neu, J. L., Parrish, D. D., Rieder, H. E., Schnell, J. L., Tilmes, S., Wild, O., Zhang, L., Ziemke, J., Brandt, J., Delcloo, A., Doherty, R. M., Geels, C., Hegglin, M. I., Hu, L., Im, U., Kumar, R., Luhar, A., Murray, L., Plummer, D., Rodriguez, J., Saiz-Lopez, A., Schultz, M. G., Woodhouse, M. T., and Zeng, G.: Tropospheric Ozone Assessment Report: Assessment of global-scale model performance for global and regional ozone distributions, variability, and trends, *Elem. Sci. Anth.*, 6, 10, <https://doi.org/10.1525/elementa.265>, 2018.
- 990 Yurganov, L. N., McMillan, W. W., Dzhola, A. V., Grechko, E. I., Jones, N. B., and van der Werf, G. R.: Global AIRS and MO-PITT CO Measurements: Validation, Comparison, and Links to Biomass Burning Variations and Carbon Cycle, *J. Geophys. Res.*, 113, <https://doi.org/10.1029/2007JD009229>, 2008.
- 995 Zhang, X., Jones, D. B. A., Keller, M., Walker, T. W., Jiang, Z., Henze, D. K., Worden, H. M., Bourassa, A. E., Degenstein, D. A., and Rochon, Y. J.: Quantifying Emissions of CO and NO_x Using Observations From MOPITT, OMI, TES, and OSIRIS, *J. Geophys. Res.*, 124, 1170–1193, <https://doi.org/10.1029/2018JD028670>, 2019.
- 1000 Zhu, C., Byrd, R. H., Lu, P., and Nocedal, J.: L-BFGS-B: A limited memory FORTRAN code for solving bound constrained optimization problems, *Tech. Rep. Tech. Rep. No. NAM-11*, EECS Dept., Northwestern Univ., Evanston, Ill, available at: <http://users.iems.northwestern.edu/nocedal/PDFfiles/lbfgsb.pdf> (last access: 2 November 2020), 1994.
- Ziemke, J. R., Chandra, S., Duncan, B. N., Froidevaux, L., Bhartia, P. K., Levelt, P. F., and Waters, J. W.: Tropospheric ozone determined from Aura OMI and MLS: Evaluation of measurements and comparison with the Global Modeling Initiative’s Chemical Transport Model, *J. Geophys. Res.*, 111, <https://doi.org/10.1029/2006JD007089>, 2006.
- 1005 Ziemke, J. R., Oman, L. D., Strode, S. A., Douglass, A. R., Olsen, M. A., McPeters, R. D., Bhartia, P. K., Froidevaux, L., Labow, G. J., Witte, J. C., Thompson, A. M., Haffner, D. P., Kramarova, N. A., Frith, S. M., Huang, L.-K., Jaross, G. R., Sefstor, C. J., Deland, M. T., and Taylor, S. L.: Trends in global tropospheric ozone inferred from a composite record of TOMS/OMI/MLS/OMPS satellite measurements and the MERRA-2 GMI simulation, *Atmos. Chem. Phys.*, 19, 3257–3269, <https://doi.org/10.5194/acp-19-3257-2019>, 2019.
- 1010 Zoogman, P., Jacob, D. J., Chance, K., Liu, X., Lin, M., Fiore, A., and Travis, K.: Monitoring high-ozone events in the US Intermountain West using TEMPO geostationary satellite observations, *Atmos. Chem. Phys.*, 14, 6261–6271, <https://doi.org/10.5194/acp-14-6261-2014>, 2014.

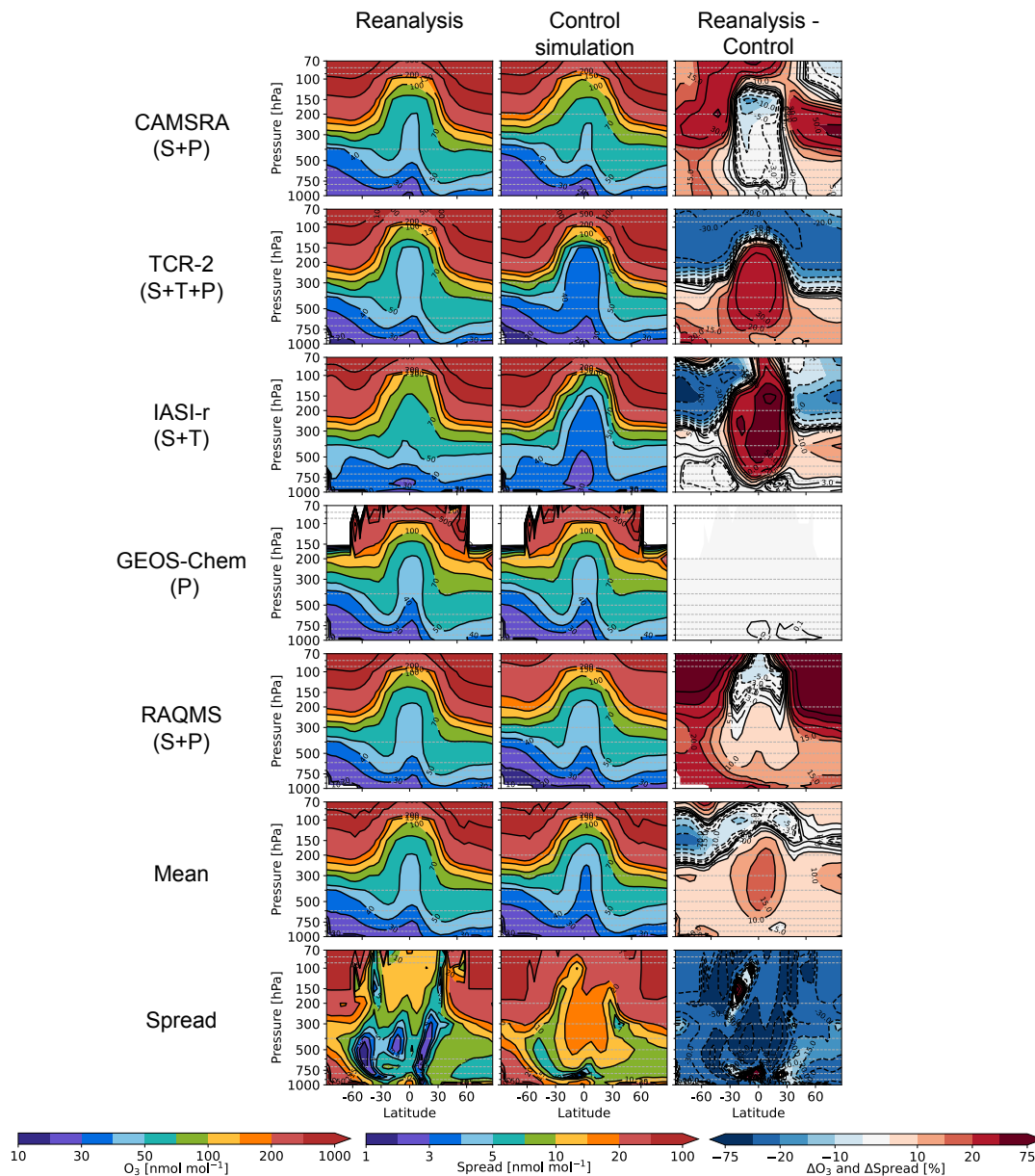


Figure 1. Latitude-pressure level cross sections of annual mean tropospheric ozone concentrations obtained from reanalysis products (top left), control simulations (middle), and their differences (bottom right) in 2010. The first through fifth columns-rows present data from CAMSRA, TCR-2, IASI-r (MOCAGE), GEOS-Chem-adjoint, and RAQMS Aura reanalysis, and the sixth and seventh columns-rows present multi-system average and spread normalized by the mean-system average data, respectively. The difference in the multi-system spread is defined as $(\text{stdev}(\text{reanalysis}) - \text{stdev}(\text{control})) / \text{stdev}(\text{control}) \times 100$, where stdev represents standard deviation. The units of ozone concentrations and the differences between reanalysis products and control simulations are mole fraction in air (nmol mol^{-1}) and percentage (%), respectively. The unit of multi-system spread is percentage (%).

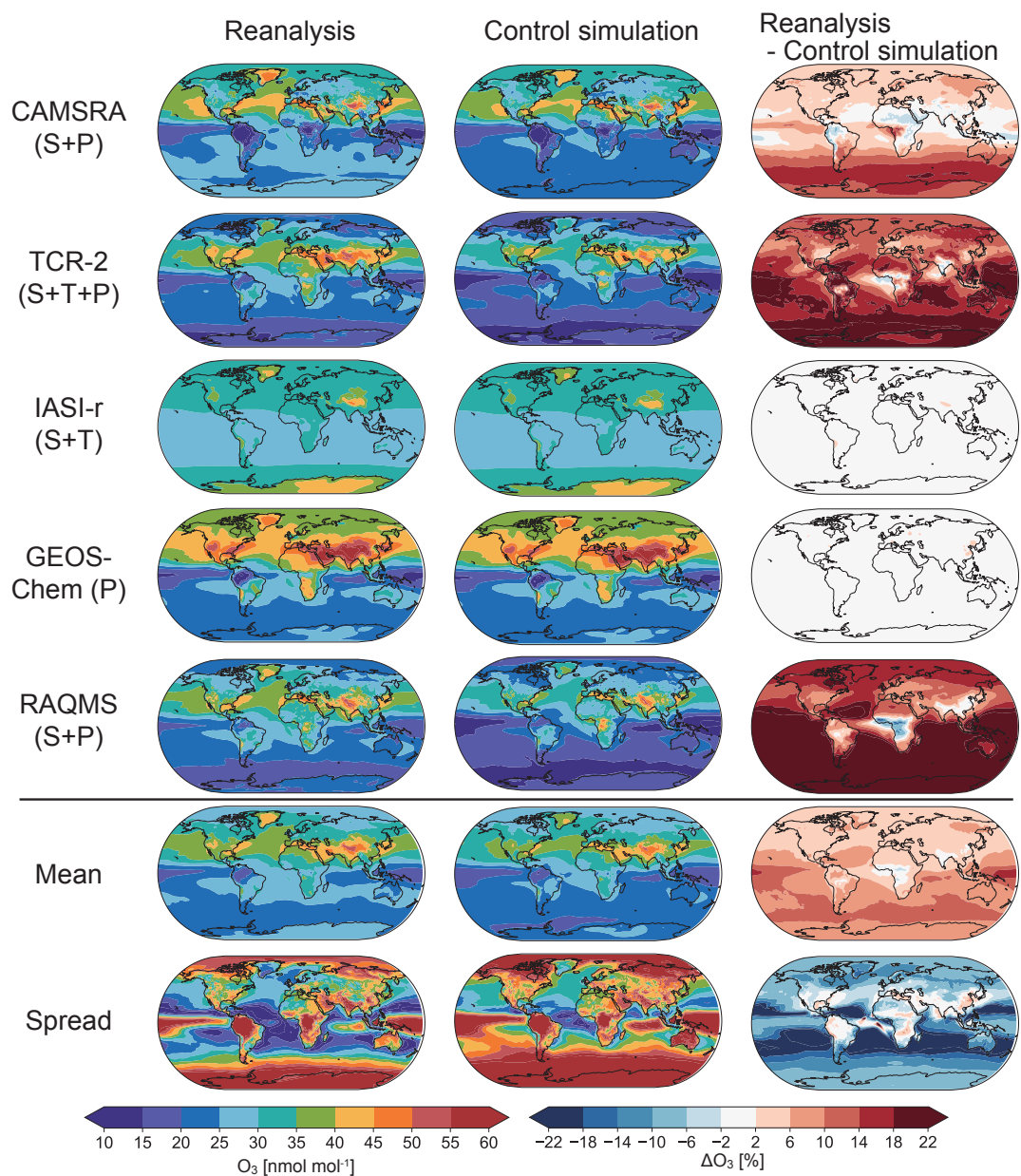


Figure 2. Global distribution of annual mean surface ozone concentrations obtained from the reanalysis products (top left), control simulations (middle), and their differences (bottom right) in 2010. The first through fifth columns represent data from CAMSRA, TCR-2, IASI-r, GEOS-Chem-adjoint, and RAQMS Aura reanalysis, and the sixth and seventh columns present multi-system average and spread normalized by the mean-system average data, respectively. The difference in the multi-system spread is defined as $(\text{stdev}(\text{reanalysis}) - \text{stdev}(\text{control})) / \text{stdev}(\text{control}) \times 100$, where stdev represents standard deviation. The units of ozone concentrations and the differences between reanalysis products and control simulations are mole fraction in air (nmol mol^{-1}) and percentage (%), respectively. The unit of multi-system spread is percentage (%).

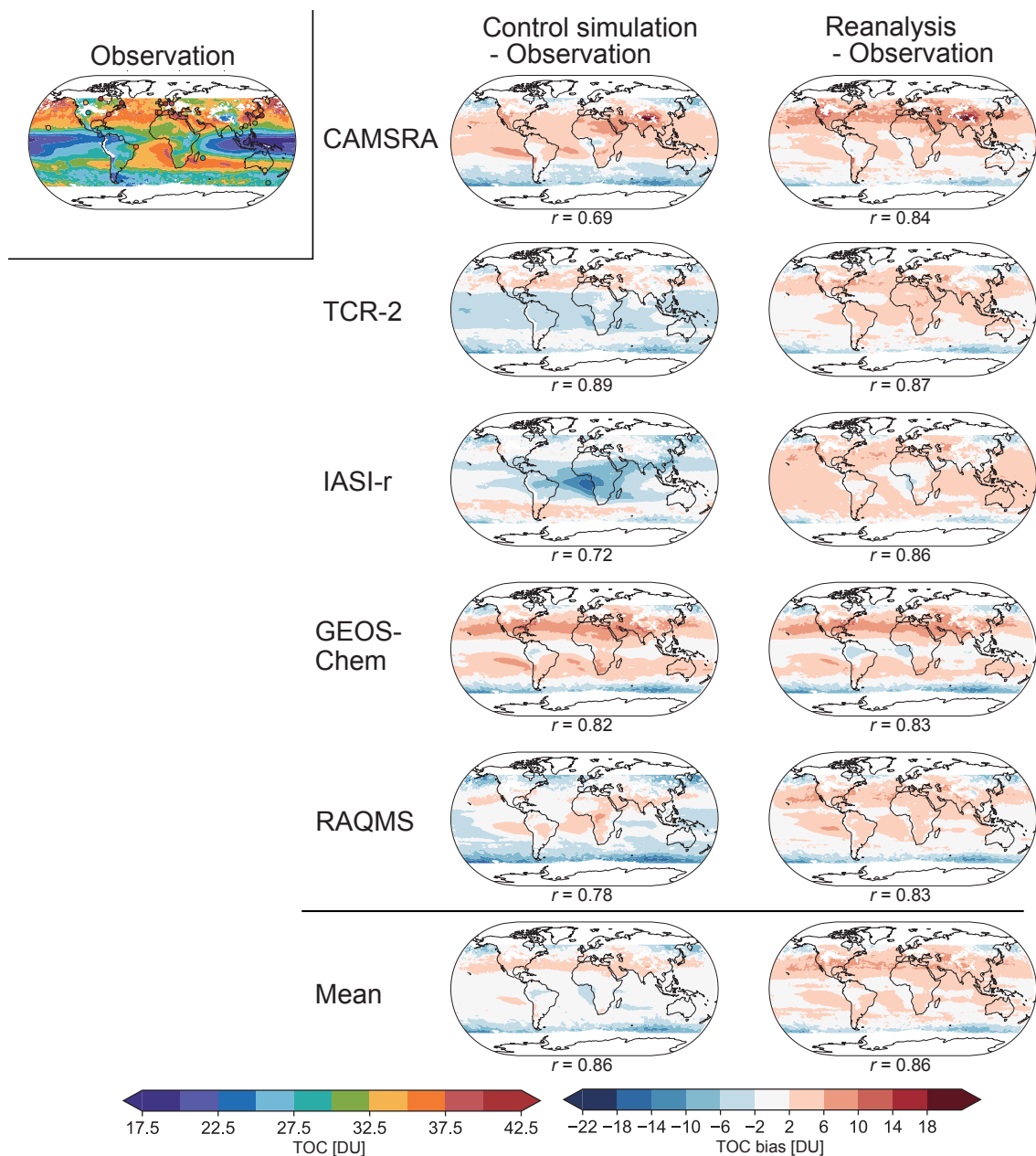


Figure 3. Global distributions of tropospheric ozone column (TOC) derived from the OMI-MLS observations [with ozonesonde measurements](#) (first column) and mean bias of the CAMSRA ([second column first row](#)), TCR-2 ([third column second row](#)), IASI-r ([fourth column third row](#)), the GEOS-Chem-adjoint ([fifth column fourth row](#)), the RAQMS Aura reanalysis ([sixth column fifth row](#)), and multi-system mean bias ([seventh column sixth row](#)) relative to OMI-MLS. [Top Second](#) and [bottom panels third columns](#) are the control simulations and reanalysis products, respectively. [We used ozonesonde measurements at the sites with more than once-per-month sampling frequency.](#) The unit is the Dobuson unit (DU). The spatial correlation coefficient (r) between OMI-MLS and the reanalysis/control simulation is also shown below the map.

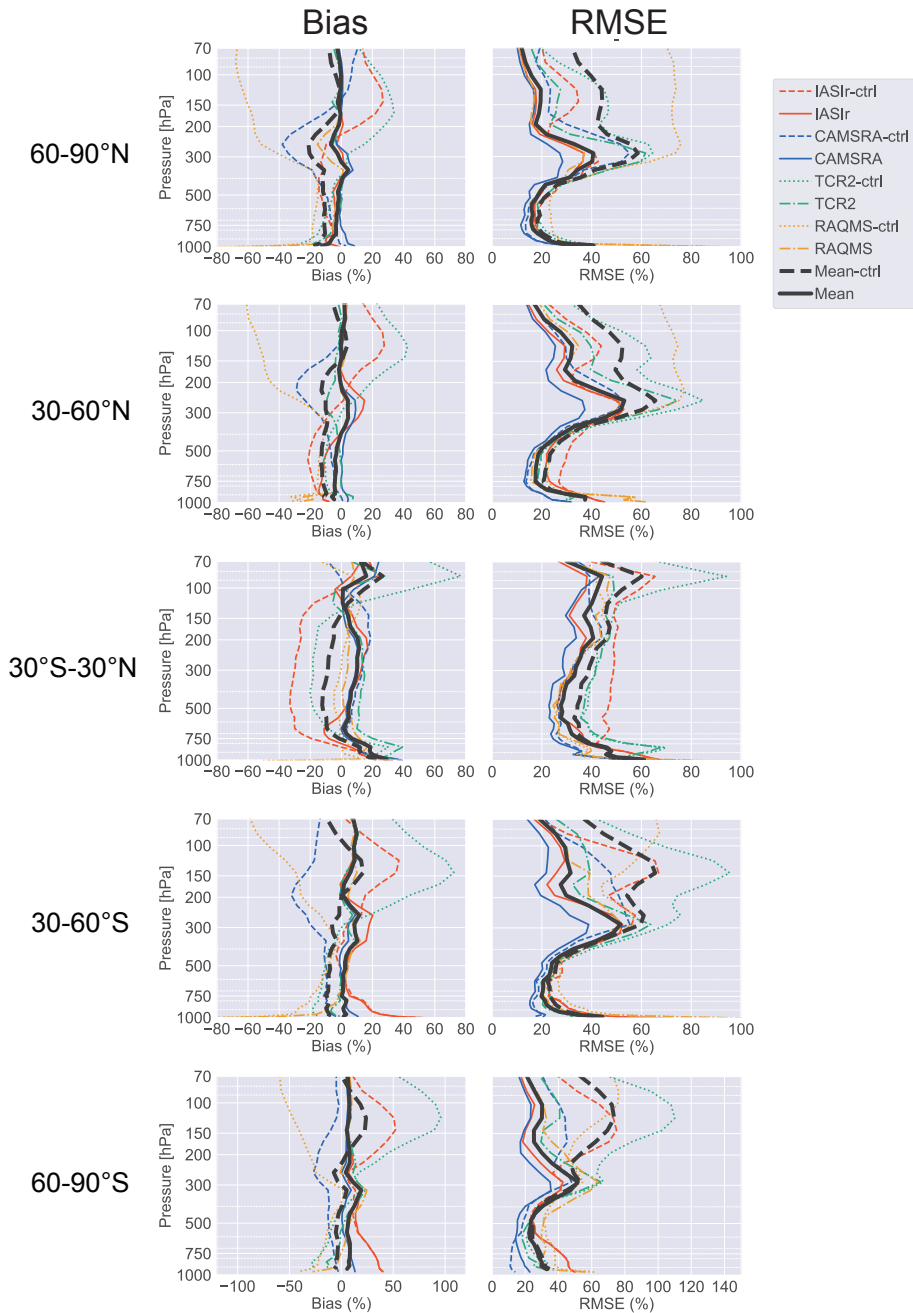


Figure 4. Vertical profiles of bias (top left) and RMSE (bottom right) for the reanalysis products and the control simulations compared to ozonesonde observations in 2010. The first through fifth columns rows present the southern-northern high latitudes (60–90°SN), the southern-northern mid-latitudes (30–60°SN), the tropics (30°S–30°N), the northern-southern mid-latitudes (30–60°NS), and the northern-southern high latitudes (60–90°NS). The blue line indicates CAMSRA, the red line indicates IASI-r, the green line indicates TCR-2, the orange line indicates the RAQMS Aura reanalysis, and the black line indicates multi-system averages. The solid and dashed-dotted lines indicate the reanalysis products, while the dashed and dotted lines indicate the control simulations, respectively. The unit is percentage (%).

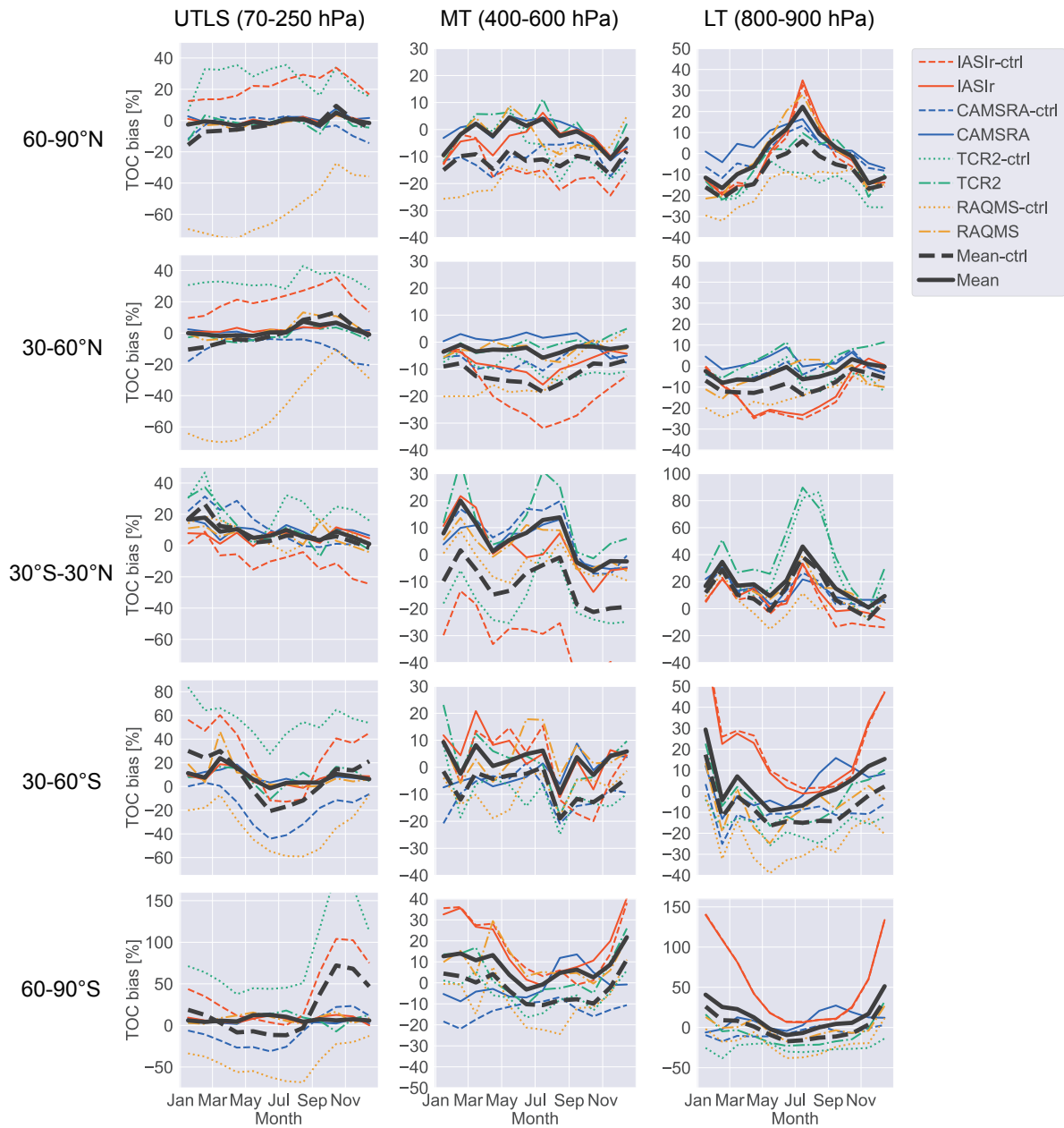
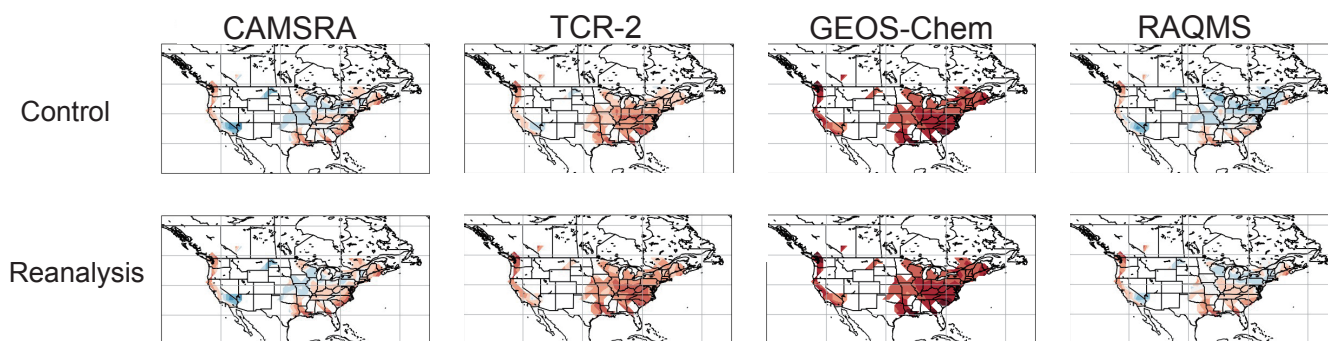
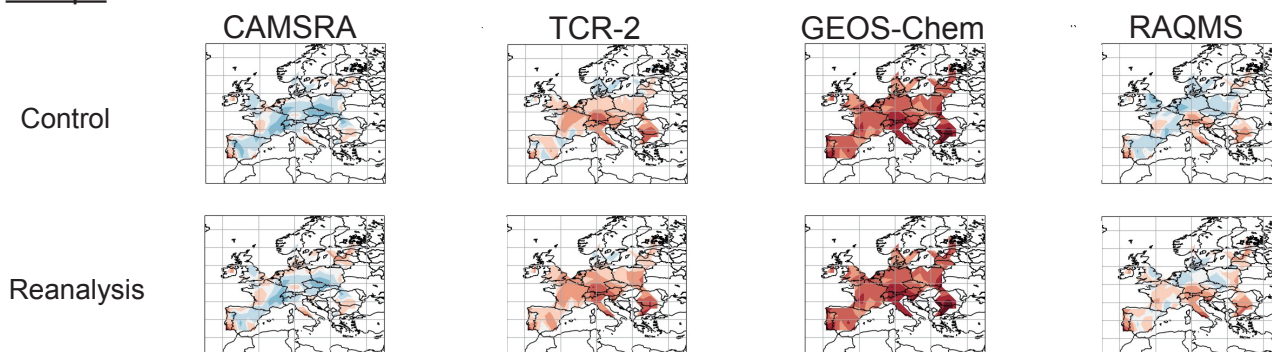


Figure 5. Monthly timeseries of bias for the reanalysis products and the control simulations compared to ozonesonde observations in 2010. The first through fifth rows present the northern high latitudes ($60\text{--}90^\circ\text{N}$), the northern mid-latitudes ($30\text{--}60^\circ\text{N}$), the tropics ($30^\circ\text{S}\text{--}30^\circ\text{N}$), the southern mid-latitudes ($30\text{--}60^\circ\text{S}$), and the southern high latitudes ($60\text{--}90^\circ\text{S}$). The first through third columns are the upper troposphere and lower stratosphere ($70\text{--}250$ hPa), middle troposphere ($400\text{--}600$ hPa), and lower troposphere ($800\text{--}900$ hPa), respectively. The blue line indicates CAMSRA, red line indicates IASIr, green line indicates TCR-2, orange line indicates the RAQMS Aura reanalysis, and black line indicates multi-system averages. The solid and dashed-dotted lines indicate the reanalysis products, while the dashed and dotted lines indicate the control simulations. The unit is percentage (%).

The United States



Europe



Northeast Asia

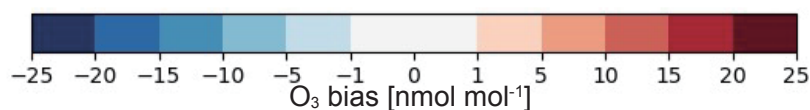
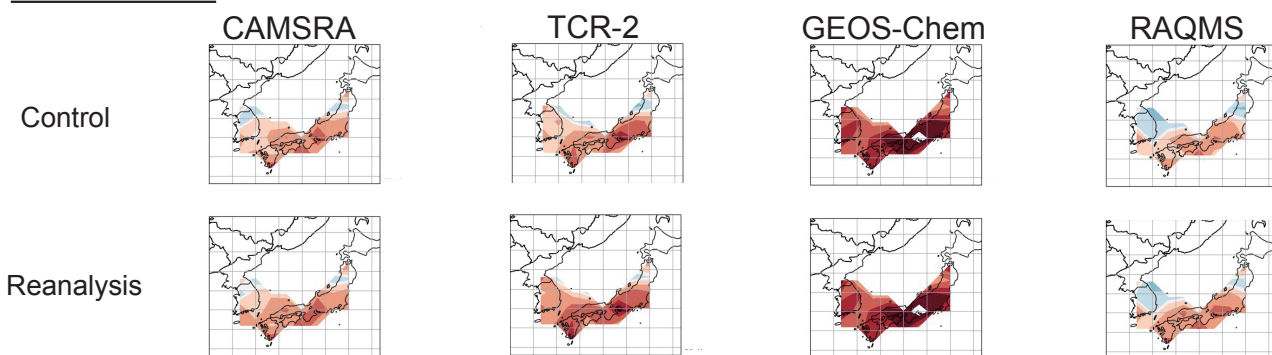


Figure 6. Bias of annual mean surface ozone relative to the TOAR database (nmol mol^{-1}) in CAMSRA (first column), TCR-2 (second column), GEOS-Chem-adjoint (third column), and the RAQMS Aura reanalysis (fourth column) in 2010. The first, third, and fifth rows are the control simulations without data assimilation, and the second, fourth, and sixth rows are the reanalysis products. The “rural_mean” aggregated data were used for the comparison. The model and reanalysis output was mapped onto the $2^\circ \times 2^\circ$ grid.

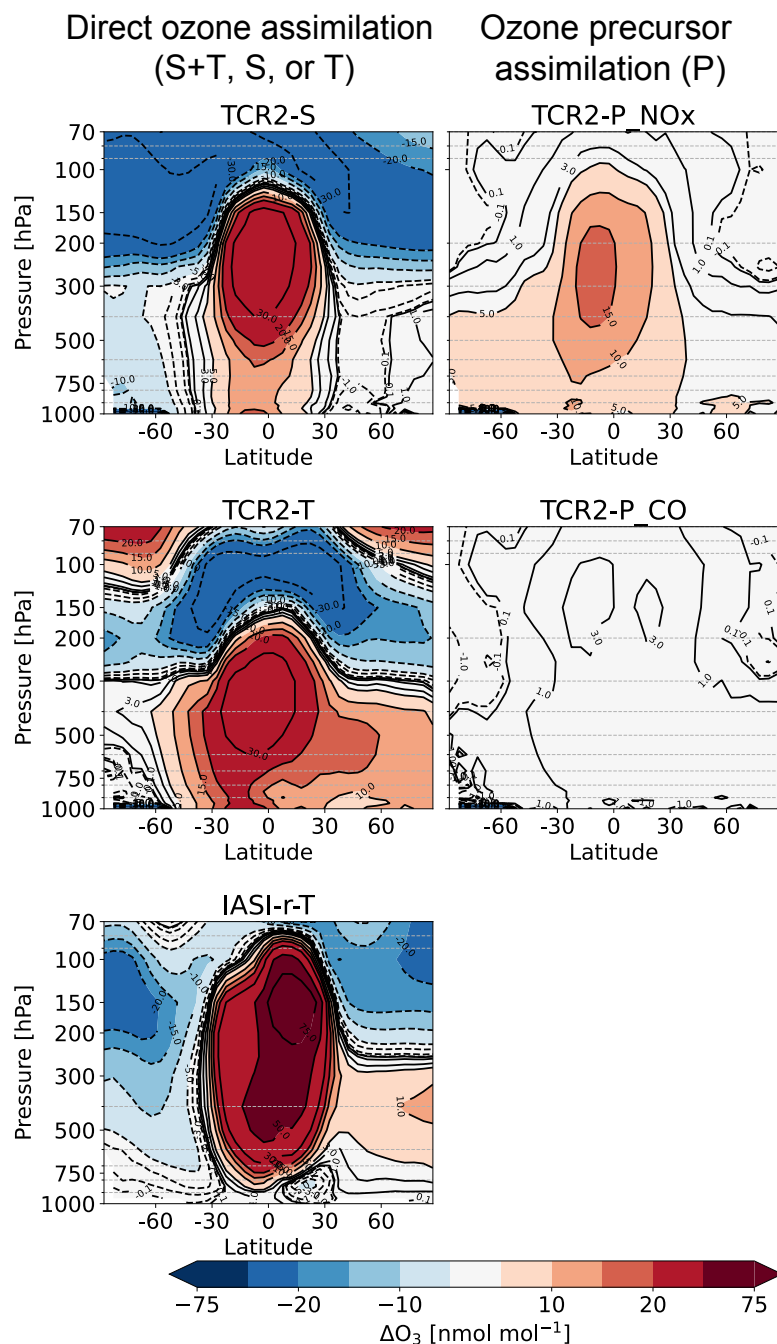


Figure 7. Latitude-pressure level cross sections of changes in annual mean ozone concentrations owing to data assimilation obtained from the OSEs in 2010. The top row presents the direct ozone assimilation (S and T): TCR-2-S (upper left), TCR-2-T (center middle left), and IASI-r-T (right bottom left); and the bottom row presents the assimilation of ozone precursors (P): TCR-2-P_NO_x (left upper right), and TCR-2-P_CO (center middle right). The units are percentage (%).

Direct ozone assimilation (S or T)

Ozone precursor assimilation (P)

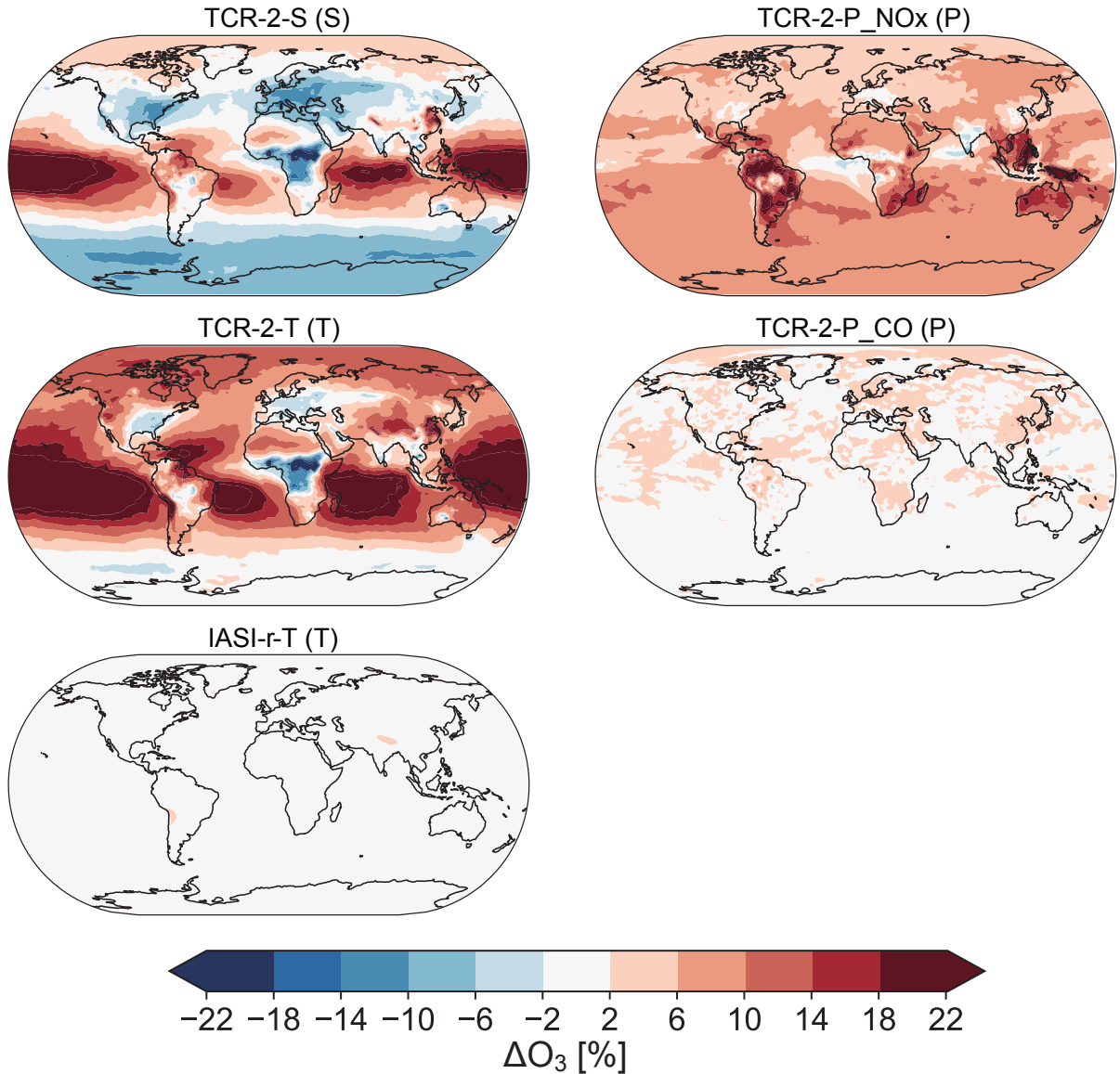


Figure 8. Global distribution of changes in annual mean surface ozone concentrations owing to data assimilation obtained from OSEs in 2010. The top row presents the direct ozone assimilation (S and T): TCR-2-S (upper left), TCR-2-T (centermiddle left), and IASI-r-T (rightbottom left); and the bottom row presents the assimilation of ozone precursors (P): TCR-2-P_NO_x (leftupper right), and TCR-2-P_CO (centermiddle right). The unit is percentage (%).

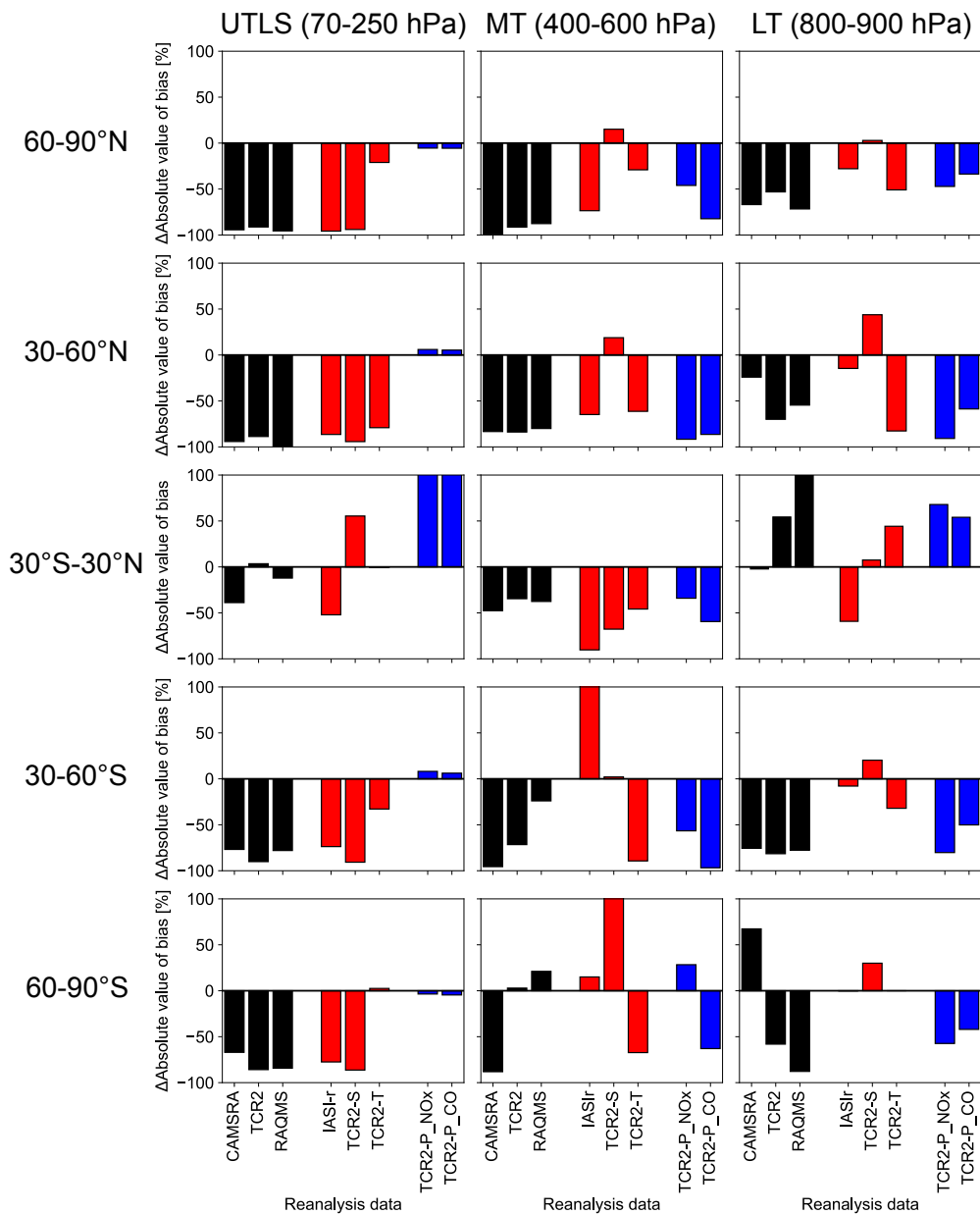


Figure 9. Relative changes in the absolute value of the mean bias (%) due to data assimilation in the reanalysis products and OSEs. These changes are calculated as follows: $(|MB_{DA}| - |MB_{CTL}|) / |MB_{CTL}| \times 100$, where MB is mean bias. **Upper row-Left column** is the upper troposphere and lower stratosphere (UTLS, 70–250 hPa), middle **row-column** is the middle troposphere (MT, 400–600 hPa), and **bottom row-right column** is the lower troposphere (LT, 800–900 hPa) in 2010. First through fifth **columns-rows** present the **southern-northern** high latitudes (60–90°**SN**), the **southern-mid-latitudes-northern mid-latitudes** (30–60°**SN**), the tropics (30°**N**–30°**S**–30°**SN**), the **northern-mid latitudes-southern mid-latitudes** (30–60°**NS**), and the **north-southern** high latitudes (60–90°**NS**). The black bars indicate the simultaneous assimilation of ozone and its precursors (S+T+P and S+P): CAMSRA, TCR-2, and the RAQMS Aura reanalysis. The red bars indicate the direct ozone assimilation (S+T, S, and T): IASIR, TCR-2-S, and TCR-2-T, and the blue bars indicate the assimilation of ozone precursors (P): TCR-2-P_NO_x and TCR-2-P_CO.

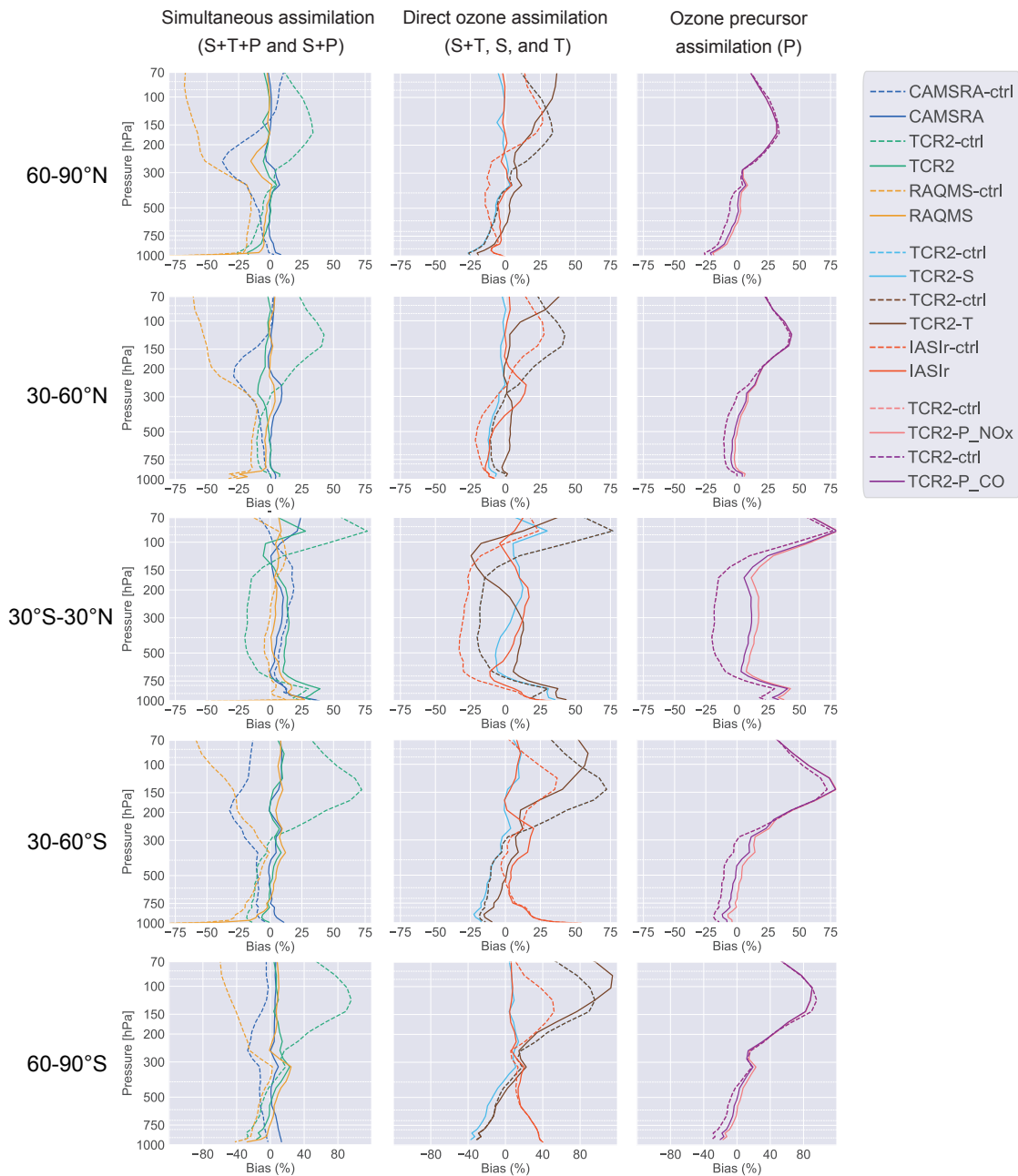


Figure 10. Vertical profiles of the bias for the data assimilation (solid lines) and the control simulations (dashed lines) relative to ozonesonde observations in 2010. **Top-Left** panels are the simultaneous assimilation (S+T+P and S+P), middle panels are the direct ozone assimilation (S+T, S, and T), and **bottom-right** panels are the ozone precursors assimilation (P). First through fifth **columns-rows** present the **southern northern** high latitudes ($60\text{--}90^\circ\text{SN}$), the **southern northern** mid-latitudes ($30\text{--}60^\circ\text{SN}$), the tropics ($30^\circ\text{S--}30^\circ\text{N}$), the **northern southern** mid-latitudes ($30\text{--}60^\circ\text{NS}$), and the **northern southern** high latitudes ($60\text{--}90^\circ\text{NS}$). The blue line indicates CAMSRA, the green line indicates TCR-2, the orange line indicates the RAQMS Aura reanalysis, the red line indicates IASI-r, the sky-blue line indicates TCR-2-S, the brown line is TCR-2-T, the pink line is TCR-2-P_NO_x, and the purple line indicates TCR-2-P_CO. The unit is percentage (%).

Table 1. List of chemical reanalysis systems used in this study.

Reanalysis system	Resolution	Scheme	Assimilated observations				Reference	
			Stratospheric ozone (S)		Tropospheric ozone (T)			Precursor gases (P)
			Total column	Profile /Partial column				
CAMSRA	$0.75^\circ \times 0.75^\circ$	4D-Var	OMI GOME2, SCIAMACHY, TROPOMI, OMPS	SBUV, MLS, MIPAS		MOPITT (CO), OMI (NO ₂)	Inness et al. (2019)	
TCR-2	$1.1^\circ \times 1.1^\circ$	EnKF		MLS	TES	MOPITT (CO), OMI, SCIAMACHY, GOME-2 (NO ₂)	Miyazaki et al. (2020a)	
IASI-r	$2^\circ \times 2^\circ$	3D-Var		MLS	IASI (L1)		Emili and El Aabaribaoune (2021)	
GEOS-Chem	$2^\circ \times 2.5^\circ$	4D-Var				OMI (NO ₂)	Qu et al. (2020)	
RAQMS	$1^\circ \times 1^\circ$	3D-Var	OMI	MLS		AIRS (CO), OMI (NO ₂)	Pierce et al. (2009)	

Table 2. List of experiments used in this study. S, T, and P represent the assimilation of satellite observations of stratospheric and tropospheric ozone and its precursors, respectively). CTL represents the control simulations without any data assimilation. X^F denotes the assimilation of full set of observations for each system.

Reanalysis	Ozone+Precursor		Ozone			Precursor		CTL
	S+T+P	S+P	S+T	S	T	P(NO ₂)	P(CO)	
CAMSRA		X^F						X
TCR-2	X^F			X	X	X	X	X
IASI-r			X^F		X			X
GEOS-Chem						X^F		X
RAQMS		X^F						X

Table 3. Mean bias (MB) ranges between different systems and root-mean-square errors (RMSEs) multi-system mean and spread for the reanalysis [control simulation in the square brackets] against ozonesonde observations in the upper troposphere (UTLS), middle troposphere (MT), and lower troposphere (LT) over five latitude bands. The unit is percentage (%).

		60–90°S	30–60°S	30°S–30°N	30–60°N	60–90°N	Global
UTLS (70–250 hPa)	MB	5–9 [-40–64]	5–7 [-32–49]	6–8 [-16–12]	-3–2 [-48–28]	-3–(-0.6) [-59–26]	-1–2 [-47–30]
	RMSE	31±8 [62±17]	30±6 [57±12]	40±5 [48±6]	31±7 [52±16]	18±4 [44±18]	30±7 [55±17]
MT (400–600 hPa)	MB	1–15 [-12–13]	-0.5–6 [-10–(-2)]	2–12 [-32–8]	-7–1 [-20–(-8)]	-4–0.4 [-16–(-5)]	-3–1 [-18–(-6)]
	RMSE	25±6 [25±4]	27±3 [28±3]	28±5 [34±8]	22±2 [26±4]	21±3 [25±2]	23±3 [28±4]
LT (800–900 hPa)	MB	-3–34 [-24–34]	-3–13 [-22–14]	2–31 [-5–20]	-14–3 [-17–(-3)]	-7–1 [-19–(-4)]	-7–3 [-14–(-2)]
	RMSE	29±10 [31±12]	22±5 [25±5]	42±10 [43±10]	22±4 [24±5]	18±3 [20±4]	25±5 [27±5]